JADE Note 144
March 15th, 2002

Determinations of α_S at $\sqrt{s} = 14$ to 44 GeV using Resummed Calculations*

Pedro A. Movilla Fernández
Max-Planck-Institut für Physik, Föhringer Ring 6, 80805 München

Abstract

This note presents a determination of the QCD strong coupling constant α_S using e^+e^- annihilation data collected by the JADE experiment at centre-of-mass energies $\sqrt{s}$ =14 to 44 GeV. The measurements are based on $\mathcal{O}(\alpha_S^2)$+NLLA QCD predictions for the event shape observables $1-T$, M_H, B_T, B_W, C and y_{23}. It turns out that resummed calculations are reliable at the lowest energies of the e^+e^- continuum although non-perturbative contributions become very important. The results,

$$\alpha_S(14.0\text{ GeV}) = 0.170^{+0.021}_{-0.017},\ \alpha_S(22.0\text{ GeV}) = 0.151^{+0.014}_{-0.012},$$
$$\alpha_S(34.8\text{ GeV}) = 0.143^{+0.012}_{-0.010},\ \alpha_S(38.3\text{ GeV}) = 0.140^{+0.011}_{-0.009}$$
$$\text{and } \alpha_S(43.8\text{ GeV}) = 0.131^{+0.010}_{-0.008},$$

are in good agreement with the QCD expectation for the running of the strong coupling constant. This is the first determination of α_S at $\sqrt{s} = 14$ and 22 GeV using the best theory calculations available so far. Data have also been used to assess the performance of various Monte Carlo generators tuned to LEP data.

This note describes preliminary JADE results.

1 Introduction

Tests of Quantum Chromodynamics (QCD) substantially benefit from e^+e^- annihilation experiments at low centre-of-mass energies $\sqrt{s}$. Several re-analyses of data collected by the JADE experiment at PETRA [1–6] demonstrate that these data represent an important counterpart to LEP w.r.t. the Z^0 peak. The JADE data used in the quoted studies were restricted to $\sqrt{s}$ = 35 GeV and 44 GeV since corresponding Monte Carlo detector simulation data were retrieved only for these energy points.

Recently, the main parts of the original JADE software were successfully resurrected, namely the tracking simulation `MCJADE` [7, 8], the JADE supervisor `SUPERV` [9] which comprises a smearing

*The content of this note is the basis for a talk contributed to „XXXVIIth Rencontres de Moriond, QCD and High Energy Hadronic Interactions“, Les Arcs, Savoie, France, March 16-23, 2002.

simulation and some standard event reconstruction algorithms, the interactive JADE graphics program JADEZ [10] and the ZE4V formatting package [11] particulary useful for studies of multihadronic final states. The software is essential to understand the impact of detector effects on the measurement of experimental observables for QCD studies down to $\sqrt{s} = 14$ GeV.

This analysis focuses on determinations of the strong coupling constant α_S from event shape observables at $\sqrt{s} = 14$ to 44 GeV using resummed $\mathcal{O}(\alpha_S^2)$+NLLA predictions [12–14] in order to stringently test the energy evolution of QCD on the basis of e^+e^- data. We complement our previous studies [1, 3] at 35 and 44 GeV by considering current Monte Carlo hadronisation models like Pythia [15, 16] and Herwig [17] and test the applicability of the perturbative theory at $\sqrt{s} = 14$ and 22 GeV where hadronisation effects become very important. The data have also been used to assess the performance of various Monte Carlo generators tuned to LEP data at such low c.m.s. energies.

The selection of the JADE data and the Monte Carlo event samples used in this analysis are described in Sect. 2. The measurement of event shape observables and the correction procedure as well as a comparison of the data with QCD event generators are outlined in Sect. 3. Sect. 4 presents a determination of the strong coupling constant based on event shape observables. In Sect. 5, we draw some conclusions.

2 Data samples and detector simulation

The studies presented here are based on data samples recorded with the JADE detector [18, 19] at $\langle\sqrt{s}\rangle$=14.0, 22.0, 34.6 (tracking '82), 35.0 (tracking '86), 38.3 and 43.8 GeV. Multihadronic events were selected by the JADE standard selection cuts [19–21] which have been summarised in detail in a previous publication [1]. The final number of events which were retained and the corresponding periods of data taking are listed in Table 1. We use the data version 9/87[1] for our standard analysis.

Corresponding Monte Carlo detector simulation data were generated using the QCD event generators Pythia 5.7/Jetset 7.4 [15,16], Ariadne 4.08 [24] and Herwig 5.9 [17]. The parameter sets used were found by tuning the corresponding model predictions to e^+e^- data collected with the OPAL experiment [25] at $\sqrt{s} = M_{Z^0}$. The tuning procedures are detailed in [26–28]. A survey of the parameter tunes of these event generators can be found e.g. in [29]. Furthermore, we also considered the predecessor version Jetset 6.3 tuned to JADE data (labelled in the following as „Jetset(J)“) since it was shown to describe e^+e^- hadronic final states (see e.g. [30, 31]). Table 2 gives a summary of the Monte Carlo samples at detector level.

Comparisons of the measured and simulated distributions of multihadronic selection cut variables and other quantities generally gave a reasonable description of the measured data. As an example, Fig. 1 shows the visible energy $E_{\rm vis} = \sum_i E_i$, the momentum balance $p_{\rm bal} = |\sum p_i^z / E_{\rm vis}|$ ($\vec{p}_i$ and E_i are the 3-momentum and the energy of the reconstructed tracks and clusters), the charged particle multiplicity distribution $n_{\rm ch}$ and the $\cos\theta_T$ distribution of the polar angle θ_T of the thrust axis at $\sqrt{s} = 14$ and 35 GeV for the different Monte Carlo models. In addition, Fig. 2 shows the normalised charged particle momentum spectrum $x_p^{(\rm ch)} = 2|\vec{p}|/\sqrt{s}$, the transverse momentum distribution w.r.t. to the sphericity axis within ($p_t^{\rm in}$) and perpendicular to the event

[1] This label refers to the „TP“ event reconstruction version roughly described e.g. in [22, 23].

$\sqrt{s}$-range	period of	run	$\mathcal{L}$	$\langle\sqrt{s}\rangle$	**multihadrons**	
[GeV]	data taking	periods	[pb^{-1}]	[GeV]	**9/87**	**5/88**
14.0	Jul.-Aug. 1981	7968-8629	1.46	**14.0**	**1734**	**1792**
22.0	Jun.-Jul. 1981	7592-7962	2.41	**22.0**	**1390**	**1408**
33.8 - 36.0	Feb. 1981 - Aug. 1982	6193-12518	61.7	**34.6**	**14372**	**14347**
35.0	Feb.-Nov. 1986	24214-30397	92.3	**35.0**	**20688**	**20925**
38.3	Oct.-Nov. 1985	23352-24187	8.28	**38.3**	**1587**	**1605**
43.4-46.6	Jun. 1984 - Oct. 1985	16803-23351	28.8	**43.8**	**3940**	**4397**

Table 1: Data samples used in this analysis for different periods of data taking. The numbers of selected events (**multihadrons**) quoted refer to the respective standard selection as described in [1,19–21]. The integrated luminosities $\mathcal{L}$ where taken from records found at DESY [32]. $\langle\sqrt{s}\rangle$ denotes the luminosity weighted mean of centre-of-mass energies $\sqrt{s}$ within a given run period.

plane (p_t^{out}) and the particle flow w.r.t the thrust axis. In most cases, the agreement is good, particulary if using PYTHIA for the event generation. It must be pointed out that some of the quantitites are sensitive to the details of the detector simulation and the event reconstruction[2]. It is expected that these details are less important for the event shape observables introduced in Sect. 3. As shown in Figs. 3 and 4 for $\sqrt{s}$ = 14, 22 and 35 GeV, the agreement of real and simulated event shape data is good, in general, if using PYTHIA or JETSET(J) for event generation. So the simulated data can be used to correct for detector effects in the measured data.

$\sqrt{s}$	detector	generated multihadrons			
[GeV]	configuration	PYTHIA 5.7	JETSET 6.3(J)	ARIADNE 4.08	HERWIG 5.9
14.0	1981	26997	27830	26964	24680
22.0	1981	29071	30563	29431	27492
34.6	1982	171584	181626	172114	156416
35.0	1986	237311	247943	238114	225197
38.3	1985	28632	30388	28763	27342
43.8	1985	68209	71643	68556	64422

Table 2: Monte Carlo samples at detector level (including ISR) used in the corrections for experimental effects. The numbers correpond to the standard multihadronic selection cuts.

[2]It cannot be excluded that some of the raw data event reconstruction steps (which are not sufficiently well documented) differ from the corresponding procedures applied in the current version of the JADE simulation and event reconstruction software (e.g. track re-fitting using a vertex constraint); this may for some quantities cause discrepancies between real and simulated data.

3 Measurement of event shapes

From the data passing the multihadronic selection criteria, the distributions of the following event shape observables were determined using the 4-momenta $(\vec{p}_i, E_i)$ of the reconstructed tracks and clusters:

- Thrust $1 - T$ [33, 34]
- Heavy jet mass M_H [35]
- Total and wide jet broadening B_T and B_W [14]
- C parameter [36, 37]
- Differential 2-jet rate y_{23} using the Durham jet resolution criterion [38].

The definitions of these observables are summarised in [1, 3].

3.1 Comparison with the JADE simulation

Figs. 3 and 4 show the measured and normalised differential distributions $1/\sigma \cdot \mathrm{d}\sigma/\mathrm{d}\mathcal{F}$ of the observables $\mathcal{F}$ at detector level at $\sqrt{s}$ = 14, 22 and 35 GeV. Also shown is the corresponding JADE simulation using the QCD event generators mentioned in Sect. 2. In general the predictions based on PYTHIA, ARIADNE and JETSET(J) agree well for all energy points and run periods. HERWIG underestimates the peak region of some distributions and exhibits an excess in the 3-jet region at high values of $\mathcal{F}$.

3.2 Correction procedure

The event shape data were corrected for the limited acceptance and resolution of the detector and for initial state photon radiation effects by applying a bin-by-bin correction procedure. Since mass effects due to the electroweak decay of heavy b-hadrons faking gluon activity in the 3-jet region are crucial at $\sqrt{s}$ = 14 and 22 GeV, we take the contribution $\mathrm{e^+e^-} \to \mathrm{b\bar{b}}$ as an additional background. Thus we take into account that the QCD calculations used for the determination of α_S are based on massless quarks.

For the correction procedure described in the following —referred to as the standard correction— the PYTHIA based JADE simulation with the multihadron selection cuts described in Sect. 2 is used to estimate the $\mathrm{b\bar{b}}$ contribution to the event shape distribution which is indicated by the shaded areas in Figs. 3 and 4. In a first step, we performed a binwise $\mathrm{b\bar{b}}$-background subtraction at detector level in order to take into account the impact of detector effects on the shape of $\mathrm{b\bar{b}}$ events. In a second step, correction factors were defined by the ratio of the distribution calculated from events generated with PYTHIA 5.7 without detector and ISR simulation (*hadron level*) over the same distribution at detector level including ISR effects. The hadron level prediction is based on light flavoured events (u, d, s and c) and comprises all particles with lifetime $\tau > 3 \cdot 10^{-10} s$. For this purpose we use the PYTHIA generator since the corresponding predictions are in good agreement with the data for all energy points mentioned here not only for the event shapes

used in the α_S analysis but also for many other quantities. Moreover, the model includes a next-to-leading-order description of QED ISR effects [16].

The applicability of a bin-by-bin unfolding method was veryfied by testing the correction procedure to HERWIG samples at detector level used as pseudo data which indeed reproduces the initial HERWIG distribution at hadron level. Furthermore we also performed a simplified matrix correction of pure detector effects combined with a bin-by-bin correction of ISR effects and observed that the resulting corrected distributions are compatible with those obtained using the bin-by-bin method. These tests indicate that the choosen bin widths of the distributions are not too small and that bin migration effects are properly taken into account.

3.3 Experimental systematic uncertainties

Systematic uncertainties to the corrected data distributions were investigated by modifying the event selection and the correction procedure. In general, we follow the procedure of our previous publication [1]. Some multihadron selection cuts were tightened compared with [1] in order to better reject background and badly reconstructed events[3]. Differently from [1], we estimated the uncertainties due to the merging of clusters and associated tracks performed by the reconstruction software by recalculating the observables using all tracks and clusters but taking cluster energies *uncorrected* for associated tracks, instead of repeating the analysis using tracks und cluster seperately. Furthermore, we also considered the preprocessed JADE data version 5/88 in order to take into account uncertainties due to event reconstruction details. A further error stems from the tune uncertainty of the parameter ϵ_b of the Peterson fragmentation function which controls the fragmentation of b quarks in the simulation and therefore is relevant for the $b\bar{b}$ background subtraction. We varied ϵ_b by the one standard deviation limits published by the OPAL collaboration [27].

Any deviation from the result obtained applying the standard correction procedure (see Sect. 3.2) was considered as systematic error. In general, the maximum deviation from the standard result for each kind of variation was regarded as symmetric systematic uncertainty. The total error was obtained by adding the individual systematic errors and the statistical error in quadrature.

3.4 Comparison with QCD Monte Carlo models

The resulting data distributions, thus corrected to hadron level, are represented by Figs. 5-10 for all observables at $\sqrt{s} = 14$, 22, 35 and 43.8 GeV. For comparison, the respective distributions predicted by PYTHIA 5.7, JETSET 6.3(J), ARIADNE 4.08, HERWIG 5.9 and COJETS 6.23 [39] at hadron level based on u, d, s, and c events are also shown. In case of PYTHIA, there is good agreement between the data and the model over the whole kinematic range of the observables. Taking the experimental uncertainties into account, the performance of ARIADNE and HERWIG is still moderate at $\sqrt{s} = 14$ GeV and improves at increasing centre-of-mass energies. In contrast to that, the JETSET(J) prediction fits the 14 GeV data but increasingly deviates from the data at higher c.m.s. energies. The prediction of COJETS is clearly disfavoured by the lower energy data and remains worse also at higher energies.

[3] The cut on the missing momentum was tightened to $p_{\mathrm{miss}} < 0.2 \cdot \sqrt{s}$, the momentum balance requirement was restricted to $p_{\mathrm{bal}} < 0.2$, and the cut for the visible energy E_{vis} was varied by $\pm 0.1 \cdot \sqrt{s}$.

The observed performance of the QCD Monte Carlo models is also reflected by other shape quantities not shown here. The LEP tuned PYTHIA generator works surprisingly well also for PETRA energies, whereas the other generators obviously need a re-tune at lower energies.

4 Determination of α_S at $\sqrt{s}$ =14 to 44 GeV

4.1 QCD predictions

The determination of the strong coupling constant α_S is based on a combination of an exact QCD matrix element calculation in $\mathcal{O}(\alpha_S^2)$ and a next-to-leading-logarithmic approximation (NLLA) for the event shape observables presented in Sect. 3. The coefficents of the $\mathcal{O}(\alpha_S^2)$ predictions are obtained by a Monte Carlo integration of the QCD matrix elements [40] in the $\overline{\rm MS}$ renormalisation scheme using the program `EVENT2` [41]. The $\mathcal{O}(\alpha_S^2)$ calculation is expected to be valid in the 3-jet region of phase space where the radiation of a single hard gluon dominates. The NLLA prediction for $1-T$ and M_H were calculated in [12], for the jet broadening B_T and B_W in [14,42], for the C parameter in [13] and for the differential 2-jet rate in [43]. The NLLA is valid in the 2-jet region of phase space where multiple radiation of soft and collinear gluons from a system of two hard back-to-back partons dominate. There are several matching schemes to combine the $\mathcal{O}(\alpha_S^2)$ and the NLLA calculations, see [12] for details. We use the so-called ln(R)-matching for the determination of the main result of α_S since it is preferred theoretically [12] as well as experimentally [44].

4.2 Measurement method

The strong coupling constant α_S was determined by χ^2 fits of the theoretical predictions to the event shape distributions corrected to hadron level, using only the statistical errors for the calculation of χ^2. During the fits, the perturbative QCD calculations introduced in Sect. 4.1 were simultaneously corrected for hadronisation effects. For the main results, we use the ln(R)-matching for the perturbative prediction with the renormalisation scale factor $x_\mu \equiv \mu/\sqrt{s}$ set to 1 and PYTHIA 5.7 for the estimation of non-perturbative contributions.

The handling of hadronisation effects in this analysis is different from the procedure described in our previous studies [1, 3] where the *differential* data distributions were corrected bin-by-bin for hadronisation effects and then directly compared with the perturbative predictions. We observed that this method does not conserve the normalisation of the data distributions in particular at $\sqrt{s} = 14$ and 22 GeV where the hadronisation correction factors become large. In the present analysis, we correct the *cumulative* theoretical distributions $R(\mathcal{F}) \equiv \int_0^{\mathcal{F}} \mathrm{d}\mathcal{F}' \frac{1}{\sigma}\frac{\mathrm{d}\sigma}{\mathrm{d}\mathcal{F}'}$ for each bin i by corresponding correction factors $K_i = R_i^{\rm had}/R_i^{\rm par}$ derived from the ratio of the corresponding *cumulative* distributions $R^{\rm had}$ at hadron level over the same distribution $R^{\rm par}$ at parton level, which were calculated from PYTHIA after and before hadronisation, respectively. This not only ensures normalisation conservation but also takes more properly into account bin migration effects which occur at $\mathcal{F}$ close to 0.

We tested the fit procedure using hadron level predictions at $\sqrt{s} = 14$ to 91 GeV from various QCD Monte Carlo generators. From a comparison of the extracted energy dependence of α_S with the two-loop expectation for the running coupling it turns out that correcting the cumulative

distributions reproduces the energy evolution of α_S explicitly implemented in the Monte Carlo models.

The choice of fit ranges for each observable were determined by choosing the largest range

1. for which the hadronisation correction is flat,
2. for which the hadronisation uncertainties described in Sect. 4.3 deviate from the standard correction by less than a factor of 0.5 to 2.0,
3. for which the χ^2 of a bin does not significantly contribute to the total χ^2 of the fit,
4. and for which the fitted α_S results are independent of the fit range.

For the sake of convergence of the fit and in order to keep the fit errors under control, it is not always possible to fulfill the demand 2, particularly at $\sqrt{s} = 14$ and 22 GeV. The fit ranges are tabulated in Tables 4-9.

4.3 Fit errors and systematic uncertainties

In principle we follow the procedure in [1] but differ in several details. Since our standard estimation of hadronisation effects is based on an OPAL tuned PYTHIA Monte Carlo, we focus on the impact of the respective tune uncertainties on the fit results instead of the tune uncertainties mentioned in [1]. Moreover, additional uncertainties due to the usage of alternative hadronisation models for the α_S fits have to be taken into account. We considered the following fit and systematic uncertainties for the α_S determination:

Fit error: This is the error returned by the fit when using statistical errors only.

Fit range: The remaining changes in α_S when enlarging or reducing the fit range by one bin on either side were taken as systematic uncertainties, if they exceed the fit error.

Experimental systematic errors: Uncertainties due to the details of the multihadron selection criteria, the merging of clusters and associated tracks and the choice of the alternative preprocessed data set (version 5/88) were considered according to the procedure explained in Sect. 3.3. The maximum deviation from the main result for each kind of variation was taken as symmetric error, except the deviation resulting from using the alternative data set which was regarded as asymmetric error.

Since the fit errors turned out to be very large for $\sqrt{s} = 14$ and 22 GeV, the experimental systematic errors at these energies were treated differently from those at other energies: We neglected any systematic uncertainties if they do not exceed the fit error, while we quadratically subtracted the fit error as estimate of the statistical component for the other systematic errors[4].

Tuning of hadronisation model parameters: The impact of the hadronisation model implemented in the PYTHIA 5.7 generator was studied by varying the values of several significant model parameters by about one standard deviation around their tuned values

[4] A more sophisticated handling of the statistical component of the experimental systematic errors is currently in progress.

from Ref. [27], namely the parameters b of the Lund symmetric fragmentation function, the width σ_q of the transverse momentum distribution, the parameters ϵ_c and ϵ_b of the Peterson fragmentation function for the heavy quarks and the parton shower cut-off value Q_0, see [15, 16] for details. It should be noted that the parameter ϵ_b is only relevant for the subtraction of the $b\bar{b}$ background described in Sect. 3.2 and affects only the hadron level corrected data distributions rather than the details of the hadronisation seen by the α_S fits, whilst the variation of ϵ_c directly affects the uncertainties of the fragmentation of c hadrons. The latter may also reflect the uncertainties of the measurements due to remaining mass effects which are not implemented in the perturbative QCD predictions. Deviations w.r.t. the standard result are considered as asymmetric error and added in quadrature in order to obtain the total error.

We also performed α_S measurements using the old JETSET 6.3 parton shower version [45, 46] optimised for the description of JADE data [30, 31] since it satisfactorily decribes the event shape data at $\sqrt{s} = 14$ and 22 GeV and is also not clearly disfavoured at higher PETRA energies. In this case, JETSET 6.3(J) samples at detector and hadron level were used for the correction of detector effects and the subtraction of the $b\bar{b}$ background. The PETRA optimisation of JETSET 6.3 yields a completely different prediction of hadronisation effects, even though the hadron level distributions are in good agreement with the PYTHIA expectation. The main reason for the tuning differences are caused by a different handling of meson multiplets with orbital momentum L=1 and by different suppression factors for diquarks in the fragmentation.

From a conservative point-of-view there is no clear evidence that the respective parameters optimised to LEP data are also valid at PETRA energies. Hence, the deviation of the α_S result obtained when using the PETRA optimisation of JETSET 6.3 from our standard result was considered a systematic error contribution. We quoted half of the observed discrepancy as symmetric error.

Since PYTHIA 5.7 and JETSET 6.3 rely on the same parton shower and string fragmentation model, we defined the larger of the two errors obtained from PYTHIA 5.7 and from JETSET 6.3(J) as total tuning uncertainty.

Choice of hadronisation model: A further systematic uncertainty comes from the choice of the hadronisation model. The analysis was repeated using ARIADNE 4.08 and HERWIG 5.9 for the correction of hadronisation effects. The COJETS 6.23 generator which uses the independent fragmentation model is not considered since it fails to describe the data in certain kinematic regions. For these checks, the respective predictions at detector and hadron level where also used to estimate detector effects and to perform the subtraction of the $b\bar{b}$ contribution to the event shape distributions. Half of the largest deviation between the fit results when using PYTHIA, HERWIG or ARIADNE was regarded as symmetric error.

Unknown higher orders: The impact of unknown higher orders of the perturbation theory on the determination of α_S were assessed by varying the renormalisation scale factor $x_\mu \equiv \mu/\sqrt{s}$ from 0.5 to 2.0. The changes in the fit results w.r.t. the standard analysis are considered as asymmetric systematic uncertainties. As a further check, we also tried the modified ln(R)-, the naive R- and the modified R- matching schemes (see [12] for details) to combine the $\mathcal{O}(\alpha_S^2)$ with the resummed NLLA calculations. A possible matching scheme uncertainty is defined by half of the largest range spanned by the results obtained from all four matching schemes mentioned in this analysis.

We took the larger of both, the renormalisation scale and the matching scheme uncertainty as error contribution.

4.4 Fit results

The fitted theoretical predictions for the ln(R)-matching and the corresponding data distributions are shown in Figs. 11-16 for all observables[5] at $\sqrt{s}$ =14, 22, 35 (tracking '86) and 43.8 GeV. We generally observe a good agreement of the resummed predictions with the data at all c.m.s. energies, indicated by the values of χ^2/d.o.f. of the fits ranging from about 0.2 and 2.0, see Tables 4-9. It is notable that for most observables, the agreement is also good in the extrapolated part of the theory curves far into the 2-jet region outside the fit ranges. For B_W, we observe a significant excess of the theory in the 3-jet region of the data, thus forcing a hard restriction of the fit range for this observable in order to get reasonable χ^2/d.o.f. in particular at $\sqrt{s}$ = 35 GeV, since a single bin would dominate the total χ^2/d.o.f.. Taking into account the fit errors, we observed that most fits are stable under variation of the fit ranges, as demonstrated by the plots on the righthand side of Figs. 11-16.

The numerical values for α_S for the standard procedure and for the systematic checks are summarised for each observable in Tables 4-9. For $\sqrt{s} > 22$ GeV, the dominant error contribution comes from renormalisation scale uncertainties indicating missing higher order terms in the perturbative prediction. The matching scheme uncertainties are well covered by the renormalisation scale uncertainties. It should be noted that the corresponding errors are much larger for the pure $\mathcal{O}(\alpha_S^2)$ calculations. At $\sqrt{s} = 14$ and 22 GeV, the tuning and hadronisation model uncertainties are in general slightly larger than the higher order errors.

The α_S results obtained when using JETSET 6.3(J) to estimate hadronisation effects are in general systematically higher than the corresponding PYTHIA 5.7 results. This is in accordance with the expectation because the size of the JETSET(J) correction is significantly smaller than the PYTHIA correction. In contrast, HERWIG and ARIADNE based hadronisation corrections yield systematically lower values for α_S. The respective χ^2/d.o.f. listed in Tables 4-9 reveal that the fits at $\sqrt{s} = 14$ and 22 GeV do not clearly prefer a certain hadronisation model. At higher energies, we observed that using the fit ranges optimised for the standard measurement, the JETSET(J) and HERWIG Monte Carlo are disfavoured for some event shape observables. But it also turns out that the fit quality for these checks can be significantly improved in many cases if the fit ranges are reduced, yielding values for α_S similar to the standard result.

The ratios of the perturbative prediction including hadronisation effects over the same prediction without hadronisation effects are shown for each generator on the righthand side of Figs. 11-16. The respective factors are rather large at $\sqrt{s} = 14$ and 22 GeV and decrease significantly at higher c.m.s. energies. This is also true for the total hadronisation uncertainties represented by the shaded bands in Figs. 11-16.

It should be noted that the fit errors obtained at $\sqrt{s}$ =14 and 22 GeV are very large compared e.g. with the fit errors obtained at 38.3 GeV, despite the fact that the data statistics are approximately equal. A variation of α_S used for the calculation of the QCD prediction excluding and including hadronisation effects, respectively, showed that the sensivity of fits on α_S are significantly reduced due to hadronisation effects.

[5]For comparison, also the R-matching prediction as well as the pure $\mathcal{O}(\alpha_S^2)$ fits with x_μ=1 and x_μ treated as additional free parameter of the fit are overlayed.

$\langle\sqrt{s}\rangle$ [GeV]	$\alpha_S(\sqrt{s})$	fit error	experimental	hadronisation	higher orders	total
14.0	0.1704	$\pm 0.0051^*$		$^{+0.0141}_{-0.0136}$	$^{+0.0143}_{-0.0091}$	$^{+0.0206}_{-0.0171}$
22.0	0.1513	$\pm 0.0043^*$		± 0.0101	$^{+0.0101}_{-0.0065}$	$^{+0.0144}_{-0.0121}$
34.6 ('82)	0.1409	± 0.0012	± 0.0017	± 0.0071	$^{+0.0086}_{-0.0057}$	$^{+0.0114}_{-0.0093}$
35.0 ('86)	0.1457	± 0.0011	± 0.0020	± 0.0076	$^{+0.0096}_{-0.0064}$	$^{+0.0125}_{-0.0101}$
38.3	0.1397	± 0.0031	± 0.0026	± 0.0054	$^{+0.0084}_{-0.0056}$	$^{+0.0108}_{-0.0087}$
43.8	0.1306	± 0.0019	± 0.0032	± 0.0056	$^{+0.0068}_{-0.0044}$	$^{+0.0096}_{-0.0080}$

Table 3: Results for α_S derived from the individual results using the weighted average method. The numbers for $\sqrt{s} = 14$ and 22 GeV marked with * represent a preliminary combined error of fit and experimental uncertainties.

4.5 Combination of the results

The α_S results derived from all event shape observables at $\sqrt{s} = 14$ to 43.8 GeV are also shown in Fig. 17. The scatter of α_S values from different event shapes is similar at all c.m.s. energies. The quadratic sum of experimental and fit errors are denoted by the solid inner error bars, the total errors including theoretical uncertainties are given by the dashed error bars. On the basis of fit and experimental errors, the individual results are consistent with each other within 1-2 standard deviations. Obviously the theoretical uncertainties become significantly smaller at increasing c.m.s. energies.

For each c.m.s. energy, the individual results of the six variables were combined using the weighted mean method described in [1] which accounts for correlations of the systematic uncertainties. The final results obtained with this procedure are listed in Table 3. For simplicity, the experimental error of the mean values were symmetrised. The fit error of the mean is given by the smallest fit error obtained by the individual fits.

The total errors are dominated by higher order uncertainties. At $\sqrt{s} = 14$ and 22 GeV, hadronisation uncertainties are very large but still at the same order of magnitude as the renormalisation scale uncertainties.

5 Summary and conclusions

This note presents a first determination of the QCD coupling α_S at $\sqrt{s} = 14$ and 22 GeV using resummed $\mathcal{O}(\alpha_S^2)$+NLLA predictions for the event shape observables $1-T$, M_H, B_T, B_W, C and y_{23}. The analysis is based on e^+e^- data collected by the JADE experiment. Due to the successful resurrection of the original JADE simulation and event reconstruction software, data at the lowest c.m.s. energies of the e^+e^- continuum became available for state-of-the-art QCD studies. We also updated our measurements presented in previous studies [1, 3] at around $\sqrt{s} =$ 35 and 44 GeV and in addition considered data at $\sqrt{s} \simeq 38$ GeV.

The values for α_S were derived from fits of the combined $\mathcal{O}(\alpha_S^2)$+NLLA predictions corrected for hadronisation effects to the differential distributions of the observables. To estimate hadroni-

sation effects, we used the QCD event generators PYTHIA 5.7, ARIADNE 4.08 and HERWIG 5.9 tuned to OPAL data and also considered JETSET 6.3 optimised to JADE data. It turned out that the PYTHIA Monte Carlo is surprisingly well capable of describing many aspects of hadronic final states in e^+e^- annihilation down to the lowest c.m.s. energies, e.g. event shapes and particle spectra, whereas the agreement of the predictions of the other generators with the data is slightly worse. In particular the HERWIG generator needs an improved tuning in order to reduce the discrepancies with the data seen at PETRA energies.

We observed that the resummed QCD theory commonly used for α_S determinations at LEP fits the data very well down to $\sqrt{s} = 14$ GeV. Nevertheless, the determination of α_S is affected by large hadronisation uncertainties at the lowest energies which are approximately of the same order of magnitude as the renormalisation scale uncertainties. But still a consistent measurement of α_S at each energy point was possible. Our final results are

$\langle\sqrt{s}\rangle$ [GeV]	$\alpha_S(\langle\sqrt{s}\rangle)$	$\alpha_S(M_{Z^0})$
14.0	$0.170^{+0.021}_{-0.017}$	$0.121^{+0.010}_{-0.009}$
22.0	$0.151^{+0.014}_{-0.012}$	$0.119^{+0.009}_{-0.008}$
34.8	$0.143^{+0.012}_{-0.010}$	$0.122^{+0.008}_{-0.007}$
38.3	$0.140^{+0.011}_{-0.009}$	$0.121^{+0.008}_{-0.007}$
43.8	$0.131^{+0.010}_{-0.008}$	$0.116^{+0.008}_{-0.006}$

where the errors quoted are the total uncertainties. The result at $\sqrt{s} = 34.8$ GeV is the weighted mean from the values derived from two different data sets at $\sqrt{s} = 34.6$ and 35.0 GeV, respectively, using the reciprocal total errors as weights. The α_S values at $\sqrt{s} \simeq 35$ and 44 GeV are compatible with those determined in our previous studies [1,3]. Using the three-loop formula for the running coupling constant [47], the values evolved to the Z^0 peak are in excellent agreement with direct measurements at $\sqrt{s} = M_{Z^0}$ and with the current world average value $\alpha_S(M_{Z^0}) = 0.118 \pm 0.003$ quoted in [48].

The results for α_S provided by this re-analysis of the JADE data are shown in Fig. 18 in comparison with the values obtained from other experiments at $\sqrt{s} = 58$ to 189 GeV basing on a similar set of event shape data and the same perturbation theory [48]. The innermost error bars denote the statistical and experimental uncertainties, the dotted error bars are the total errors. The solid line represents the energy evolution of α_S as predicted by QCD using the world average value mentioned above. The measurements agree with the QCD expectation even within the experimental and statistical uncertainties. Only these errors should be taken into account for this test since the theoretical errors are strongly correlated. A χ^2 fit of the $\mathcal{O}(\alpha_S^3)$ QCD prediction for five active flavours to the data yields $\alpha_S(M_{Z^0}) = 0.1213 \pm 0.0006$ with a χ^2/d.o.f. of 8.3/11. The hypothesis of a constant value of α_S is disfavoured by the measurements even if the theoretical uncertainties are taken into account. In this case, a fit gives $\alpha_S = 0.1174 \pm 0.0020$ and a χ^2/d.o.f. = 43.1/11 that corresponds to a fit probability of $\approx 10^{-5}$. The JADE data significantly improve the verification of the QCD expectation on basis on e^+e^- data.

Acknowledgements

I am grateful to O. Biebel and J. Olsson for helpful comments and for proof reading this manuscript.

References

[1] JADE Coll., P. A. Movilla Fernández, O. Biebel, S. Bethke et al., Eur. Phys. J. **C1** (1998), 461–478.

[2] JADE and OPAL Coll., P. Pfeifenschneider, O. Biebel, P. A. Movilla Fernández et al., Eur. Phys. J. **C17** (2000), 19–51.

[3] JADE Coll., O. Biebel, P. A. Movilla Fernández, and S. Bethke, Phys. Lett. **B459** (1999), 326–334.

[4] S. Kluth, P. A. Movilla Fernández, S. Bethke, C. Pahl, and P. Pfeifenschneider, Eur. Phys. J. **C21** (2001), 199–210.

[5] P. A. Movilla Fernández, S. Bethke, O. Biebel, and S. Kluth, Eur. Phys. J. **C22** (2001), 1–15.

[6] JADE Coll., M. Blumenstengel, O. Biebel, P. A. Movilla Fernández et al., Phys. Lett. **B517** (2001), 37–46.

[7] E. Elsen, *Detector Monte Carlo*, JADE Computer Note 54.

[8] E. Elsen, *Multihadronerzeugung in der e^+e^--Vernichtung bei PETRA-Energien und Vergleich mit Aussagen der Quantenchromodynamik.* PhD thesis, Universität Hamburg, 1981.

[9] C. Bowdery and J. Olsson, *The JADE SUPERVISOR Program.* JADE Computer Note 73.

[10] C. Bowdery and J. Olsson, *JADEZ - The JADE Graphics Program.* JADE Computer Note 85/D.

[11] G. Eckerlin and M. Zimmer, *A New Compact Data-Format Description of Bank ZE4V.* JADE Computer Note 99.

[12] S. Catani, L. Trentadue, G. Turnock, and B. R. Webber, Nucl. Phys. **B407** (1993), 3–42.

[13] S. Catani and B. R. Webber, Phys. Lett. **B427** (1998), 377–384.

[14] S. Catani, G. Turnock, and B. R. Webber, Phys. Lett. **B295** (1992), 269–276.

[15] Torbjörn Sjöstrand, Comput. Phys. Commun. **82** (1994), 74–90.

[16] Torbjörn Sjöstrand, *PYTHIA 5.7 and JETSET 7.4 Physics and Manual.* CERN-TH-7112-93.

[17] G. Marchesini et al., Comput. Phys. Commun. **67** (1992), 465–508.

[18] B. Naroska, Phys. Rept. **148** (1987), 67.

[19] JADE Coll., W. Bartel et al., Phys. Lett. **B88** (1979), 171.

[20] JADE Coll., W. Bartel et al., Phys. Lett. **B129** (1983), 145.

[21] JADE Coll., S. Bethke et al., Phys. Lett. **B213** (1988), 235.

[22] W. Bartel, *Minutes of the JADE Software Meeting on Dec. 14, 1987 at DESY.* JADE Computer Note 98.

[23] C.K. Bowdery and J.J. Pryce, *The New TP Program Version 9.* JADE Computer Note 102.

[24] Leif Lönnblad, Comput. Phys. Commun. **71** (1992), 15–31.

[25] OPAL Coll., K. Ahmet et al., Nucl. Instrum. Meth. **A305** (1991), 275–319.

[26] OPAL Coll., M. Z. Akrawy et al., Z. Phys. **C47** (1990), 505–522.

[27] OPAL Coll., G. Alexander et al., Z. Phys. **C69** (1996), 543–560.

[28] Hemingway, R.J., *An OPAL Tune of HERWIG using Z^0 Data.* OPAL Technical Note TN652, April 2000.

[29] I. G. Knowles et al., *QCD Event Generators.* hep-ph/9601212, 1995.

[30] M. Zimmer, *Die Fragmentation von b-Quarks.* PhD thesis, Ruprecht-Karls-Universität, Heidelberg, 1989.

[31] G. Eckerlin, *Vergleich der starken Wechselwirkung von b-Quarks und leichten Quarks in e^+e^--Reaktionen bei 35 GeV.* PhD thesis, Ruprecht-Karls-Universität, Heidelberg, 1990.

[32] J. Olsson, private communication, 1999.

[33] S. Brandt, C. Peyrou, R. Sosnowski, and A. Wroblewski, Phys. Lett. **12** (1964), 57–61.

[34] Edward Farhi, Phys. Rev. Lett. **39** (1977), 1587–1588.

[35] T. Chandramohan and L. Clavelli, Nucl. Phys. **B184** (1981), 365.

[36] G. Parisi, Phys. Lett. **B74** (1978), 65.

[37] John F. Donoghue, F. E. Low, and So-Young Pi, Phys. Rev. **D20** (1979), 2759.

[38] S. Catani, Yuri L. Dokshitzer, M. Olsson, G. Turnock, and B. R. Webber, Phys. Lett. **B269** (1991), 432–438.

[39] R. Odorico, Comput. Phys. Commun. **72** (1992), 238–248.

[40] R. K. Ellis, D. A. Ross, and A. E. Terrano, Nucl. Phys. **B178** (1981), 421.

[41] S. Catani and M. H. Seymour, Phys. Lett. **B378** (1996), 287–301.

[42] Yuri L. Dokshitzer, A. Lucenti, G. Marchesini, and G. P. Salam, JHEP **01** (1998), 11.

[43] Günther Dissertori and Michael Schmelling, Phys. Lett. **B361** (1995), 167–178.

[44] OPAL Coll., P. D. Acton et al., Z. Phys. **C59** (1993), 1–20.

[45] Torbjörn Sjöstrand, Comput. Phys. Commun. **39** (1986), 347.

[46] Torbjörn Sjöstrand and Mats Bengtsson, Comput. Phys. Commun. **43** (1987), 367.

[47] Particle Data Group, D. E. Groom et al., Eur. Phys. J. **C15** (2000) 1.

[48] S. Bethke, J. Phys. **G26** (2000), R27.

Tables

	T	M_H	B_T	B_W	C	y_{23}
fit range	0.12-0.32	0.30-0.50	0.16-0.30	0.10-0.20	0.34-0.72	0.010-0.200
α_s**(14.0 GeV)**	**0.1697**	**0.1758**	**0.1691**	**0.1566**	**0.1594**	**0.1912**
(χ^2/d.o.f.)	(3.6/6)	(3.6/4)	(1.6/5)	(3.0/4)	(10.0/5)	(5.8/7)
fit + experimental	$\pm$**0.0106**	$\pm$**0.0095**	$\pm$**0.0092**	$\pm$**0.0051**	$\pm$**0.0131**	$\pm$**0.0054**
hadronization	$^{+\mathbf{0.0198}}_{-\mathbf{0.0191}}$	$^{+\mathbf{0.0126}}_{-\mathbf{0.0124}}$	$\pm$**0.0169**	$\pm$**0.0113**	$^{+\mathbf{0.0275}}_{-\mathbf{0.0270}}$	$\pm$**0.0161**
higher orders	$^{+\mathbf{0.0175}}_{-\mathbf{0.0132}}$	$^{+\mathbf{0.0156}}_{-\mathbf{0.0112}}$	$^{+\mathbf{0.0194}}_{-\mathbf{0.0148}}$	$^{+\mathbf{0.0116}}_{-\mathbf{0.0083}}$	$^{+\mathbf{0.0139}}_{-\mathbf{0.0103}}$	$^{+\mathbf{0.0124}}_{-\mathbf{0.0076}}$
total error	$^{+\mathbf{0.0266}}_{-\mathbf{0.0234}}$	$^{+\mathbf{0.0224}}_{-\mathbf{0.0194}}$	$^{+\mathbf{0.0269}}_{-\mathbf{0.0238}}$	$^{+\mathbf{0.0170}}_{-\mathbf{0.0150}}$	$^{+\mathbf{0.0312}}_{-\mathbf{0.0292}}$	$^{+\mathbf{0.0205}}_{-\mathbf{0.0179}}$
$\cos\theta_T$	$\pm$0.0017	$\pm$0.0037	$\pm$0.0060	$\pm$0.0029	$\pm$0.0052	$\pm$0.0034
p_{miss}	$\pm$0.0028	$\pm$0.0043	$\pm$0.0016	$\pm$0.0010	$\pm$0.0009	$\pm$0.0011
p_{bal}	$\pm$0.0023	$\pm$0.0034	$\pm$0.0021	$\pm$0.0023	$\pm$0.0016	$\pm$0.0020
E_{vis}	$\pm$0.0007	$\pm$0.0012	$\pm$0.0023	$\pm$0.0012	$\pm$0.0011	$\pm$0.0005
$N_{\mathrm{ch}} > 7$	$-$0.0010	+0.0014	+0.0003	+0.0002	$-$0.0015	$-$0.0001
Tracks/Clusters	+0.0003	+0.0002	$-$0.0037	$-$0.0011	$-$0.0068	$-$0.0054
data version	+0.0114	+0.0058	+0.0013	+0.0015	+0.0052	+0.0017
fit range	$\pm$0.0029	$\pm$0.0109	$\pm$0.0102	$\pm$0.0060	$\pm$0.0189	$\pm$0.0042
MC stat.	$\pm$0.0029	$\pm$0.0028	$\pm$0.0026	$\pm$0.0014	$\pm$0.0026	$\pm$0.0015
$b - 1\sigma$	$-$0.0060	$-$0.0029	$-$0.0044	$-$0.0015	$-$0.0063	$-$0.0016
$b + 1\sigma$	+0.0049	+0.0026	+0.0036	+0.0019	+0.0050	+0.0021
$\sigma_q - 1\sigma$	+0.0058	+0.0021	+0.0047	+0.0025	+0.0060	+0.0031
$\sigma_q + 1\sigma$	$-$0.0055	$-$0.0019	$-$0.0048	$-$0.0022	$-$0.0060	$-$0.0029
$\epsilon_c - 1\sigma$	+0.0090	+0.0041	+0.0071	+0.0023	+0.0134	+0.0037
$\epsilon_c + 1\sigma$	$-$0.0073	$-$0.0023	$-$0.0067	$-$0.0012	$-$0.0125	$-$0.0027
$\epsilon_b - 1\sigma$	$-$0.0021	+0.0007	$-$0.0016	$-$0.0001	$-$0.0008	< 0.0001
$\epsilon_b + 1\sigma$	+0.0019	$-$0.0005	+0.0014	+0.0001	+0.0004	$-$0.0001
$Q_0 - 1\sigma$	$-$0.0035	$-$0.0040	+0.0018	$-$0.0014	$-$0.0044	$-$0.0038
$Q_0 + 1\sigma$	+0.0046	+0.0032	+0.0011	+0.0013	+0.0062	+0.0027
Jetset 6.3 (JADE)	+0.0231	+0.0102	+0.0222	+0.0082	+0.0208	$-$0.0021
(χ^2/d.o.f.)	(3.3/6)	(3.3/4)	(3.0/5)	(11.1/4)	(9.5/5)	(10.2/7)
Ariadne 4.08	$-$0.0298	$-$0.0088	$-$0.0223	$-$0.0112	$-$0.0435	$-$0.0235
(χ^2/d.o.f.)	(6.4/6)	(5.4/4)	(2.2/5)	(1.6/4)	(9.6/5)	(1.9/7)
Herwig 5.9	$-$0.0249	$-$0.0213	$-$0.0249	$-$0.0209	$-$0.0204	$-$0.0297
(χ^2/d.o.f.)	(4.8/6)	(1.6/4)	(5.1/5)	(4.5/4)	(19.8/5)	(3.7/7)
mod. ln(R)-matchaing	+0.0029	+0.0033	+0.0130	+0.0069	+0.0125	+0.0012
R-matching	+0.0017	+0.0028	$-$0.0004	+0.0024	$-$0.0013	$-$0.0135
mod. R-matching	+0.0015	+0.0015	+0.0074	+0.0021	+0.0067	+0.0017
renormalisation scale	$^{+0.0175}_{-0.0132}$	$^{+0.0156}_{-0.0112}$	$^{+0.0194}_{-0.0148}$	$^{+0.0116}_{-0.0083}$	$^{+0.0139}_{-0.0103}$	$^{+0.0124}_{-0.0025}$

Table 4: Values of $\alpha_S(14.0\,\mathrm{GeV})$ derived using $\mathcal{O}(\alpha_S^2)$+NLLA QCD predictions with the ln(R)-matching scheme for the six event shape observables. In addition, statistical and systematic uncertainties are given. The signed values indicate the direction in which the results change w.r.t. the standard analysis.

	T	M_H	B_T	B_W	C	y_{23}
fit range	0.12-0.32	0.22-0.50	0.12-0.30	0.08-0.20	0.28-0.72	0.006-0.200
α_s(22.0 GeV)	**0.1575**	**0.1477**	**0.1465**	**0.1421**	**0.1454**	**0.1679**
(χ^2/d.o.f.)	(1.6/6)	(5.4/6)	(2.0/7)	(4.9/5)	(4.1/6)	(5.3/8)
fit + experimental	**$\pm$0.0074**	**$\pm$0.0065**	**$\pm$0.0065**	**$\pm$0.0045**	**$\pm$0.0082**	**$\pm$0.0046**
hadronization	**$\pm$0.0151**	**$^{+0.0102}_{-0.0101}$**	**$\pm$0.0126**	**$\pm$0.0090**	**$\pm$0.0113**	**$\pm$0.0105**
higher orders	**$^{+0.0142}_{-0.0108}$**	**$^{+0.0084}_{-0.0055}$**	**$^{+0.0129}_{-0.0101}$**	**$^{+0.0089}_{-0.0064}$**	**$^{+0.0114}_{-0.0088}$**	**$^{+0.0087}_{-0.0062}$**
total error	**$^{+0.0208}_{-0.0187}$**	**$^{+0.0146}_{-0.0130}$**	**$^{+0.0183}_{-0.0164}$**	**$^{+0.0138}_{-0.0124}$**	**$^{+0.0164}_{-0.0147}$**	**$^{+0.0136}_{-0.0126}$**
$\cos\theta_T$	$\pm$0.0023	$\pm$0.0031	$\pm$0.0021	$\pm$0.0025	$\pm$0.0022	$\pm$0.0003
p_{miss}	$\pm$0.0024	$\pm$0.0003	$\pm$0.0017	$\pm$0.0016	$\pm$0.0012	$\pm$0.0016
p_{bal}	$\pm$0.0006	$\pm$0.0013	$\pm$0.0007	$\pm$0.0003	$\pm$0.0018	$\pm$0.0005
E_{vis}	$\pm$0.0019	$\pm$0.0027	$\pm$0.0019	$\pm$0.0015	$\pm$0.0011	$\pm$0.0009
$N_{\mathrm{ch}} > 7$	$-$0.0011	$+$0.0013	$-$0.0006	$-$0.0006	$-$0.0017	$-$0.0012
Tracks/Clusters	$-$0.0006	$+$0.0033	$+$0.0002	$+$0.0010	$-$0.0041	$+$0.0015
data version	$+$0.0034	$+$0.0034	$-$0.0005	$+$0.0009	$-$0.0002	$-$0.0011
fit range	$\pm$0.0033	$\pm$0.0061	$\pm$0.0028	$\pm$0.0058	$\pm$0.0047	$\pm$0.0025
MC stat.	$\pm$0.0017	$\pm$0.0015	$\pm$0.0015	$\pm$0.0010	$\pm$0.0018	$\pm$0.0011
$b - 1\sigma$	$-$0.0023	$-$0.0016	$-$0.0023	$-$0.0010	$-$0.0032	$-$0.0012
$b + 1\sigma$	$+$0.0023	$+$0.0017	$+$0.0016	$+$0.0005	$+$0.0029	$+$0.0005
$\sigma_q - 1\sigma$	$+$0.0023	$+$0.0009	$+$0.0021	$+$0.0010	$+$0.0025	$+$0.0013
$\sigma_q + 1\sigma$	$-$0.0021	$-$0.0008	$-$0.0026	$-$0.0011	$-$0.0032	$-$0.0010
$\epsilon_c - 1\sigma$	$+$0.0013	$+$0.0007	$+$0.0016	$+$0.0003	$+$0.0019	$+$0.0004
$\epsilon_c + 1\sigma$	$-$0.0009	$-$0.0001	$-$0.0016	$-$0.0004	$-$0.0024	$-$0.0006
$\epsilon_b - 1\sigma$	$+$0.0019	$+$0.0019	$+$0.0011	$+$0.0008	$+$0.0009	$+$0.0006
$\epsilon_b + 1\sigma$	$-$0.0016	$-$0.0015	$-$0.0009	$-$0.0009	$-$0.0005	$-$0.0006
$Q_0 - 1\sigma$	$+$0.0003	$-$0.0014	$+$0.0020	$-$0.0013	< 0.0001	$-$0.0035
$Q_0 + 1\sigma$	$+$0.0002	$+$0.0017	$-$0.0016	$+$0.0007	$+$0.0007	$+$0.0016
Jetset 6.3 (JADE)	$+$0.0127	$+$0.0041	$+$0.0153	$+$0.0018	$+$0.0171	$-$0.0045
(χ^2/d.o.f.)	(0.4/6)	(7.0/6)	(3.4/7)	(11.6/5)	(7.7/6)	(4.7/8)
Ariadne 4.08	$-$0.0113	$-$0.0053	$-$0.0096	$-$0.0073	$-$0.0088	$-$0.0143
(χ^2/d.o.f.)	(1.3/6)	(3.3/6)	(1.6/7)	(2.7/5)	(3.0/6)	(5.4/8)
Herwig 5.9	$-$0.0273	$-$0.0191	$-$0.0200	$-$0.0176	$-$0.0143	$-$0.0204
(χ^2/d.o.f.)	(1.2/6)	(3.2/6)	(4.6/7)	(6.8/5)	(11.5/6)	(3.6/8)
mod. ln(R)-matching	$+$0.0029	$+$0.0035	$+$0.0091	$+$0.0037	$+$0.0026	$+$0.0004
R-matching	$+$0.0016	$+$0.0012	$+$0.0011	$+$0.0039	$+$0.0043	$-$0.0116
mod. R-matching	$+$0.0016	$+$0.0021	$+$0.0053	$+$0.0003	$-$0.0013	$+$0.0007
renormalisation scale	$^{+0.0142}_{-0.0108}$	$^{+0.0084}_{-0.0055}$	$^{+0.0129}_{-0.0101}$	$^{+0.0089}_{-0.0064}$	$^{+0.0114}_{-0.0088}$	$^{+0.0087}_{-0.0017}$

Table 5: Values of $\alpha_S(22.0\,\mathrm{GeV})$ derived using $\mathcal{O}(\alpha_S^2)$+NLLA QCD predictions with the ln(R)-matching scheme for the six event shape observables. In addition, statistical and systematic uncertainties are given. The signed values indicate the direction in which the results change w.r.t. the standard analysis.

	T	M_H	B_T	B_W	C	y_{23}
fit range	0.14-0.32	0.22-0.46	0.12-0.30	0.08-0.18	0.28-0.72	0.004-0.200
α_s(34.6 GeV)	**0.1424**	**0.1406**	**0.1397**	**0.1339**	**0.1400**	**0.1486**
(χ^2/d.o.f.)	(13.7/5)	(10.4/5)	(6.1/7)	(6.3/4)	(1.2/6)	(12.8/9)
fit error	**$\pm$0.0020**	**$\pm$0.0018**	**$\pm$0.0015**	**$\pm$0.0012**	**$\pm$0.0019**	**$\pm$0.0012**
experimental	**$\pm$0.0025**	**$\pm$0.0023**	**$\pm$0.0021**	**$\pm$0.0021**	**$\pm$0.0029**	**$\pm$0.0019**
hadronization	**$\pm$0.0088**	**$\pm$0.0051**	**$\pm$0.0089**	**$\pm$0.0066**	**$\pm$0.0112**	**$\pm$0.0078**
higher orders	**$^{+0.0105}_{-0.0080}$**	**$^{+0.0083}_{-0.0059}$**	**$^{+0.0114}_{-0.0090}$**	**$^{+0.0080}_{-0.0059}$**	**$^{+0.0108}_{-0.0085}$**	**$^{+0.0060}_{-0.0052}$**
total error	**$^{+0.0141}_{-0.0122}$**	**$^{+0.0102}_{-0.0083}$**	**$^{+0.0147}_{-0.0129}$**	**$^{+0.0106}_{-0.0091}$**	**$^{+0.0159}_{-0.0143}$**	**$^{+0.0101}_{-0.0097}$**
$\cos\theta_T$	$\pm$0.0014	$\pm$0.0009	$\pm$0.0010	$\pm$0.0011	$\pm$0.0011	$\pm$0.0011
p_{miss}	$\pm$0.0007	$\pm$0.0001	$\pm$0.0007	$\pm$0.0007	$\pm$0.0007	$\pm$0.0006
p_{bal}	$\pm$0.0005	$\pm$0.0001	$\pm$0.0003	$\pm$0.0001	$\pm$0.0013	$\pm$0.0004
E_{vis}	$\pm$0.0008	$\pm$0.0010	$\pm$0.0009	$\pm$0.0009	$\pm$0.0010	$\pm$0.0008
$N_{\mathrm{ch}} > 7$	$-$0.0001	$-$0.0002	+0.0001	$<$ 0.0001	$<$ 0.0001	$-$0.0002
Tracks/Clusters	$-$0.0006	$-$0.0001	$-$0.0005	+0.0002	+0.0003	$-$0.0003
data version	+0.0016	+0.0013	+0.0013	+0.0011	+0.0021	+0.0010
fit range	$\pm$0.0014	$\pm$0.0021	$\pm$0.0016	$\pm$0.0015	$\pm$0.0007	$\pm$0.0014
MC stat.	$\pm$0.0006	$\pm$0.0005	$\pm$0.0005	$\pm$0.0004	$\pm$0.0006	$\pm$0.0004
$b - 1\sigma$	$-$0.0010	$-$0.0012	$-$0.0012	$-$0.0008	$-$0.0016	$-$0.0003
$b + 1\sigma$	+0.0008	+0.0013	+0.0007	+0.0003	+0.0012	+0.0003
$\sigma_q - 1\sigma$	+0.0007	+0.0006	+0.0011	+0.0005	+0.0012	+0.0006
$\sigma_q + 1\sigma$	$-$0.0007	$-$0.0006	$-$0.0012	$-$0.0008	$-$0.0015	$-$0.0003
$\epsilon_c - 1\sigma$	$<$ 0.0001	+0.0001	+0.0005	$-$0.0001	+0.0002	$-$0.0001
$\epsilon_c + 1\sigma$	$-$0.0001	$<$ 0.0001	$-$0.0005	$-$0.0002	$-$0.0004	+0.0001
$\epsilon_b - 1\sigma$	+0.0003	+0.0005	+0.0008	+0.0005	+0.0012	+0.0005
$\epsilon_b + 1\sigma$	$-$0.0003	$-$0.0006	$-$0.0006	$-$0.0004	$-$0.0008	$-$0.0003
$Q_0 - 1\sigma$	+0.0008	$-$0.0010	+0.0008	$-$0.0009	$<$ 0.0001	$-$0.0024
$Q_0 + 1\sigma$	$-$0.0005	+0.0009	$-$0.0011	+0.0004	$<$ 0.0001	+0.0017
Jetset 6.3 (JADE)	+0.0108	+0.0043	+0.0096	+0.0029	+0.0097	$-$0.0022
(χ^2/d.o.f.)	(11.6/5)	(26.2/5)	(27.5/7)	(23.3/4)	(8.6/6)	(8.4/9)
Ariadne 4.08	$-$0.0052	$-$0.0054	$-$0.0063	$-$0.0065	$-$0.0084	$-$0.0087
(χ^2/d.o.f.)	(9.2/5)	(7.2/5)	(3.9/7)	(5.5/4)	(2.9/6)	(8.5/9)
Herwig 5.9	$-$0.0139	$-$0.0093	$-$0.0150	$-$0.0128	$-$0.0201	$-$0.0150
(χ^2/d.o.f.)	(19.0/5)	(9.0/5)	(10.6/7)	(2.0/4)	(15.1/6)	(3.1/9)
mod. ln(R)-matching	+0.0033	+0.0010	+0.0061	+0.0014	$-$0.0011	+0.0002
R-matching	+0.0007	+0.0030	+0.0025	+0.0059	+0.0078	$-$0.0099
mod. R-matching	+0.0022	+0.0001	+0.0031	$-$0.0013	$-$0.0041	+0.0005
renormalisation scale	$^{+0.0105}_{-0.0080}$	$^{+0.0083}_{-0.0059}$	$^{+0.0114}_{-0.0090}$	$^{+0.0080}_{-0.0059}$	$^{+0.0108}_{-0.0085}$	$^{+0.0060}_{-0.0010}$

Table 6: Values of α_S(34.6 GeV) (tracking '82) derived using $\mathcal{O}(\alpha_S^2)$+NLLA QCD predictions with the ln(R)-matching scheme for the six event shape observables. In addition, statistical and systematic uncertainties are given. The signed values indicate the direction in which the results change w.r.t. the standard analysis.

	T	M_H	B_T	B_W	C	y_{23}
fit range	0.14-0.32	0.22-0.42	0.12-0.30	0.08-0.16	0.28-0.72	0.004-0.200
α_s**(35.0 GeV)**	**0.1461**	**0.1462**	**0.1429**	**0.1387**	**0.1439**	**0.1527**
(χ^2/d.o.f.)	(6.2/5)	(9.5/4)	(14.2/7)	(3.0/3)	(10.8/6)	(23.5/9)
fit error	**±0.0017**	**±0.0016**	**±0.0013**	**±0.0012**	**±0.0016**	**±0.0011**
experimental	**±0.0038**	**±0.0031**	**±0.0030**	**±0.0030**	**±0.0029**	**±0.0019**
hadronization	**±0.0085**	**±0.0059**	**±0.0090**	**±0.0074**	**±0.0109**	**±0.0079**
higher orders	**+0.0113 −0.0086**	**+0.0099 −0.0072**	**+0.0120 −0.0095**	**+0.0094 −0.0071**	**+0.0117 −0.0092**	**+0.0065 −0.0055**
total error	**+0.0147 −0.0125**	**+0.0120 −0.0098**	**+0.0154 −0.0133**	**+0.0124 −0.0107**	**+0.0163 −0.0144**	**+0.0105 −0.0100**
$\cos\theta_T$	±0.0004	±0.0002	±0.0005	±0.0006	±0.0002	±0.0005
p_{miss}	±0.0007	±0.0004	±0.0005	±0.0002	±0.0006	±0.0005
p_{bal}	±0.0023	±0.0003	±0.0016	±0.0011	±0.0011	±0.0001
E_{vis}	±0.0004	±0.0005	±0.0006	±0.0006	±0.0006	±0.0002
$N_{\mathrm{ch}} > 7$	+0.0004	+0.0002	+0.0006	+0.0004	+0.0005	+0.0003
Tracks/Clusters	+0.0002	−0.0011	−0.0002	−0.0006	−0.0003	−0.0008
data version	+0.0029	+0.0017	+0.0021	+0.0007	+0.0024	+0.0006
fit range	±0.0017	±0.0027	±0.0017	±0.0028	±0.0009	±0.0017
MC stat.	±0.0006	±0.0005	±0.0005	±0.0004	±0.0005	±0.0004
$b - 1\sigma$	−0.0008	−0.0011	−0.0013	−0.0004	−0.0016	−0.0003
$b + 1\sigma$	+0.0004	+0.0012	+0.0008	+0.0008	+0.0012	+0.0006
$\sigma_q - 1\sigma$	+0.0007	+0.0005	+0.0010	+0.0008	+0.0012	+0.0004
$\sigma_q + 1\sigma$	−0.0007	−0.0004	−0.0011	−0.0006	−0.0011	−0.0003
$\epsilon_c - 1\sigma$	+0.0002	+0.0003	+0.0005	+0.0001	+0.0004	−0.0002
$\epsilon_c + 1\sigma$	< 0.0001	−0.0001	−0.0004	−0.0001	−0.0003	+0.0002
$\epsilon_b - 1\sigma$	+0.0002	+0.0005	+0.0007	+0.0005	+0.0011	+0.0003
$\epsilon_b + 1\sigma$	−0.0003	−0.0005	−0.0007	−0.0005	−0.0009	−0.0004
$Q_0 - 1\sigma$	+0.0006	−0.0011	+0.0007	−0.0006	< 0.0001	−0.0022
$Q_0 + 1\sigma$	−0.0004	+0.0007	−0.0010	+0.0002	+0.0001	+0.0016
Jetset 6.3 (JADE)	+0.0092	+0.0052	+0.0091	+0.0029	+0.0088	−0.0028
(χ^2/d.o.f.)	(4.6/5)	(21.6/4)	(56.3/7)	(22.0/3)	(25.1/6)	(15.8/9)
Ariadne 4.08	−0.0046	−0.0039	−0.0058	−0.0064	−0.0079	−0.0087
(χ^2/d.o.f.)	(5.0/5)	(8.0/4)	(6.0/7)	(1.9/3)	(3.2/6)	(14.5/9)
Herwig 5.9	−0.0142	−0.0105	−0.0156	−0.0144	−0.0199	−0.0154
(χ^2/d.o.f.)	(17.9/5)	(2.8/4)	(30.8/7)	(2.9/3)	(20.2/6)	(7.5/9)
mod. ln(R)-matching	+0.0035	+0.0005	+0.0063	+0.0003	−0.0009	+0.0001
R-matching	+0.0008	+0.0039	+0.0026	+0.0081	+0.0080	−0.0105
mod. R-matching	+0.0023	−0.0004	+0.0032	−0.0025	−0.0042	+0.0005
renormalisation scale	+0.0113 −0.0086	+0.0099 −0.0072	+0.0120 −0.0095	+0.0094 −0.0071	+0.0117 −0.0092	+0.0065 −0.0012

Table 7: Values of $\alpha_S(35.0\ \mathrm{GeV})$ (tracking '86) derived using $\mathcal{O}(\alpha_S^2)$+NLLA QCD predictions with the ln(R)-matching scheme for the six event shape observables. In addition, statistical and systematic uncertainties are given. The signed values indicate the direction in which the results change w.r.t. the standard analysis.

	T	M_H	B_T	B_W	C	y_{23}
fit range	0.12-0.32	0.18-0.50	0.10-0.30	0.08-0.23	0.22-0.72	0.004-0.200
α_s**(38.3 GeV)**	**0.1508**	**0.1450**	**0.1378**	**0.1297**	**0.1395**	**0.1460**
(χ^2/d.o.f.)	(3.3/6)	(5.5/7)	(5.7/8)	(3.5/6)	(5.6/7)	(9.1/9)
fit error	**±0.0052**	**±0.0044**	**±0.0044**	**±0.0031**	**±0.0052**	**±0.0038**
experimental	**±0.0045**	**±0.0052**	**±0.0029**	**±0.0030**	**±0.0066**	**±0.0026**
hadronization	**±0.0071**	**±0.0040**	**±0.0070**	**±0.0044**	**±0.0093**	**±0.0065**
higher orders	**+0.0124 −0.0095**	**+0.0089 −0.0063**	**+0.0109 −0.0086**	**+0.0067 −0.0047**	**+0.0109 −0.0087**	**+0.0061 −0.0055**
total error	**+0.0159 −0.0137**	**+0.0119 −0.0100**	**+0.0140 −0.0123**	**+0.0091 −0.0075**	**+0.0166 −0.0152**	**+0.0100 −0.0098**
$\cos\theta_T$	±0.0018	±0.0017	±0.0014	±0.0011	±0.0034	±0.0007
p_{miss}	±0.0019	±0.0017	±0.0008	±0.0009	±0.0020	±0.0006
p_{bal}	±0.0020	±0.0017	±0.0017	±0.0011	±0.0009	±0.0016
E_{vis}	±0.0008	±0.0007	±0.0002	±0.0002	±0.0012	±0.0003
$N_{\text{ch}} > 7$	+0.0011	+0.0006	+0.0006	+0.0004	+0.0005	+0.0009
Tracks/Clusters	−0.0022	−0.0008	−0.0007	−0.0009	−0.0031	+0.0009
data version	−0.0005	+0.0016	+0.0014	+0.0022	−0.0001	+0.0011
fit range	±0.0055	±0.0052	±0.0028	±0.0020	±0.0063	±0.0028
MC stat.	±0.0013	±0.0011	±0.0011	±0.0008	±0.0013	±0.0009
$b - 1\sigma$	−0.0010	−0.0006	−0.0009	−0.0002	−0.0009	−0.0004
$b + 1\sigma$	+0.0006	+0.0008	+0.0008	+0.0002	+0.0008	+0.0003
$\sigma_q - 1\sigma$	+0.0007	+0.0003	+0.0010	+0.0003	+0.0010	+0.0004
$\sigma_q + 1\sigma$	−0.0008	−0.0002	−0.0011	−0.0003	−0.0010	−0.0005
$\epsilon_c - 1\sigma$	+0.0001	+0.0001	+0.0004	< 0.0001	+0.0001	−0.0002
$\epsilon_c + 1\sigma$	−0.0002	+0.0001	−0.0004	< 0.0001	−0.0002	+0.0001
$\epsilon_b - 1\sigma$	+0.0004	+0.0005	+0.0009	+0.0003	+0.0012	+0.0005
$\epsilon_b + 1\sigma$	−0.0001	−0.0003	−0.0005	−0.0002	−0.0008	−0.0002
$Q_0 - 1\sigma$	+0.0003	−0.0005	+0.0008	−0.0007	+0.0005	−0.0023
$Q_0 + 1\sigma$	−0.0004	+0.0004	−0.0010	+0.0006	−0.0004	+0.0016
Jetset 6.3 (JADE)	+0.0090	+0.0028	+0.0088	+0.0010	+0.0093	−0.0033
(χ^2/d.o.f.)	(3.3/6)	(5.8/7)	(2.9/8)	(6.1/6)	(3.3/7)	(12.4/9)
Ariadne 4.08	−0.0033	−0.0026	−0.0042	−0.0049	−0.0055	−0.0070
(χ^2/d.o.f.)	(3.0/6)	(5.8/7)	(6.8/8)	(5.1/6)	(7.8/7)	(17.1/9)
Herwig 5.9	−0.0107	−0.0071	−0.0108	−0.0085	−0.0159	−0.0125
(χ^2/d.o.f.)	(3.7/6)	(4.0/7)	(6.0/8)	(4.0/6)	(5.3/7)	(16.4/9)
mod. ln(R)-matching	+0.0027	+0.0016	+0.0039	+0.0029	−0.0029	−0.0001
R-matching	+0.0015	+0.0028	+0.0037	+0.0041	+0.0089	−0.0110
mod. R-matching	+0.0016	+0.0006	+0.0014	+0.0001	−0.0056	< 0.0001
renormalisation scale	+0.0124 −0.0095	+0.0089 −0.0063	+0.0109 −0.0086	+0.0067 −0.0047	+0.0109 −0.0087	+0.0061 −0.0015

Table 8: Values of $\alpha_S(38.3\,\text{GeV})$ derived using $\mathcal{O}(\alpha_S^2)$+NLLA QCD predictions with the ln(R)-matching scheme for the six event shape observables. In addition, statistical and systematic uncertainties are given. The signed values indicate the direction in which the results change w.r.t. the standard analysis.

	T	M_H	B_T	B_W	C	y_{23}
fit range	0.10-0.32	0.14-0.50	0.10-0.30	0.06-0.23	0.22-0.72	0.002-0.200
α_s**(43.8 GeV)**	**0.1349**	**0.1317**	**0.1300**	**0.1222**	**0.1322**	**0.1394**
(χ^2/d.o.f.)	(7.0/7)	(6.3/8)	(6.9/8)	(12.4/7)	(5.4/7)	(11.2/10)
fit error	**±0.0031**	**±0.0022**	**±0.0026**	**±0.0019**	**±0.0031**	**±0.0020**
experimental	**±0.0055**	**±0.0029**	**±0.0034**	**±0.0030**	**±0.0046**	**±0.0036**
hadronization	**±0.0076**	**±0.0050**	**±0.0073**	**±0.0043**	**±0.0087**	**±0.0065**
higher orders	**+0.0090 −0.0070**	**+0.0068 −0.0048**	**+0.0094 −0.0074**	**+0.0054 −0.0037**	**+0.0093 −0.0073**	**+0.0049 −0.0044**
total error	**+0.0134 −0.0118**	**+0.0092 −0.0078**	**+0.0126 −0.0113**	**+0.0078 −0.0068**	**+0.0138 −0.0125**	**+0.0092 −0.0088**
$\cos\theta_T$	±0.0001	±0.0014	±0.0017	±0.0011	±0.0007	±0.0013
p_{miss}	±0.0044	±0.0016	±0.0017	±0.0020	±0.0032	±0.0021
p_{bal}	±0.0006	±0.0003	±0.0008	±0.0002	±0.0010	±0.0001
E_{vis}	±0.0021	±0.0018	±0.0021	±0.0013	±0.0017	±0.0015
$N_{\text{ch}} > 7$	−0.0004	−0.0005	−0.0006	−0.0007	−0.0006	−0.0005
Tracks/Clusters	+0.0004	−0.0001	+0.0002	+0.0004	+0.0012	+0.0010
data version	+0.0024	+0.0008	+0.0001	+0.0003	+0.0021	+0.0017
fit range	±0.0022	±0.0021	±0.0031	±0.0023	±0.0027	±0.0016
MC stat.	±0.0007	±0.0006	±0.0007	±0.0005	±0.0008	±0.0005
$b - 1\sigma$	−0.0006	−0.0015	−0.0007	−0.0003	−0.0009	−0.0001
$b + 1\sigma$	+0.0007	+0.0014	+0.0006	+0.0003	+0.0008	+0.0004
$\sigma_q - 1\sigma$	+0.0008	+0.0007	+0.0010	+0.0003	+0.0009	+0.0004
$\sigma_q + 1\sigma$	−0.0007	−0.0007	−0.0008	−0.0005	−0.0008	−0.0004
$\epsilon_c - 1\sigma$	+0.0002	+0.0002	+0.0004	−0.0001	+0.0002	+0.0001
$\epsilon_c + 1\sigma$	+0.0001	−0.0002	−0.0001	< 0.0001	< 0.0001	+0.0002
$\epsilon_b - 1\sigma$	+0.0005	+0.0009	+0.0008	+0.0004	+0.0009	+0.0005
$\epsilon_b + 1\sigma$	< 0.0001	−0.0003	−0.0003	−0.0001	−0.0003	−0.0002
$Q_0 - 1\sigma$	+0.0006	−0.0007	+0.0009	−0.0008	+0.0003	−0.0021
$Q_0 + 1\sigma$	−0.0002	+0.0006	−0.0008	+0.0005	−0.0002	+0.0016
Jetset 6.3 (JADE)	+0.0092	+0.0057	+0.0088	+0.0022	+0.0096	−0.0017
(χ^2/d.o.f.)	(9.1/7)	(19.8/8)	(11.3/8)	(26.7/7)	(3.9/7)	(9.3/10)
Ariadne 4.08	−0.0028	−0.0012	−0.0028	−0.0026	−0.0037	−0.0064
(χ^2/d.o.f.)	(6.9/7)	(7.4/8)	(7.0/8)	(7.2/7)	(7.4/7)	(10.4/10)
Herwig 5.9	−0.0121	−0.0080	−0.0115	−0.0083	−0.0144	−0.0126
(χ^2/d.o.f.)	(4.9/7)	(4.6/8)	(4.3/8)	(3.6/7)	(6.1/7)	(6.7/10)
mod. ln(R)-matching	+0.0023	+0.0011	+0.0048	+0.0025	−0.0016	< 0.0001
R-matching	+0.0010	+0.0028	+0.0025	+0.0033	+0.0074	−0.0085
mod. R-matching	+0.0015	+0.0004	+0.0024	+0.0001	−0.0041	+0.0004
renormalisation scale	+0.0090 −0.0070	+0.0068 −0.0048	+0.0094 −0.0074	+0.0054 −0.0037	+0.0093 −0.0073	+0.0049 −0.0007

Table 9: Values of $\alpha_S(43.8\,\text{GeV})$ derived using $\mathcal{O}(\alpha_S^2)$+NLLA QCD predictions with the ln(R)-matching scheme for the six event shape observables. In addition, statistical and systematic uncertainties are given. The signed values indicate the direction in which the results change w.r.t. the standard analysis.

Figures

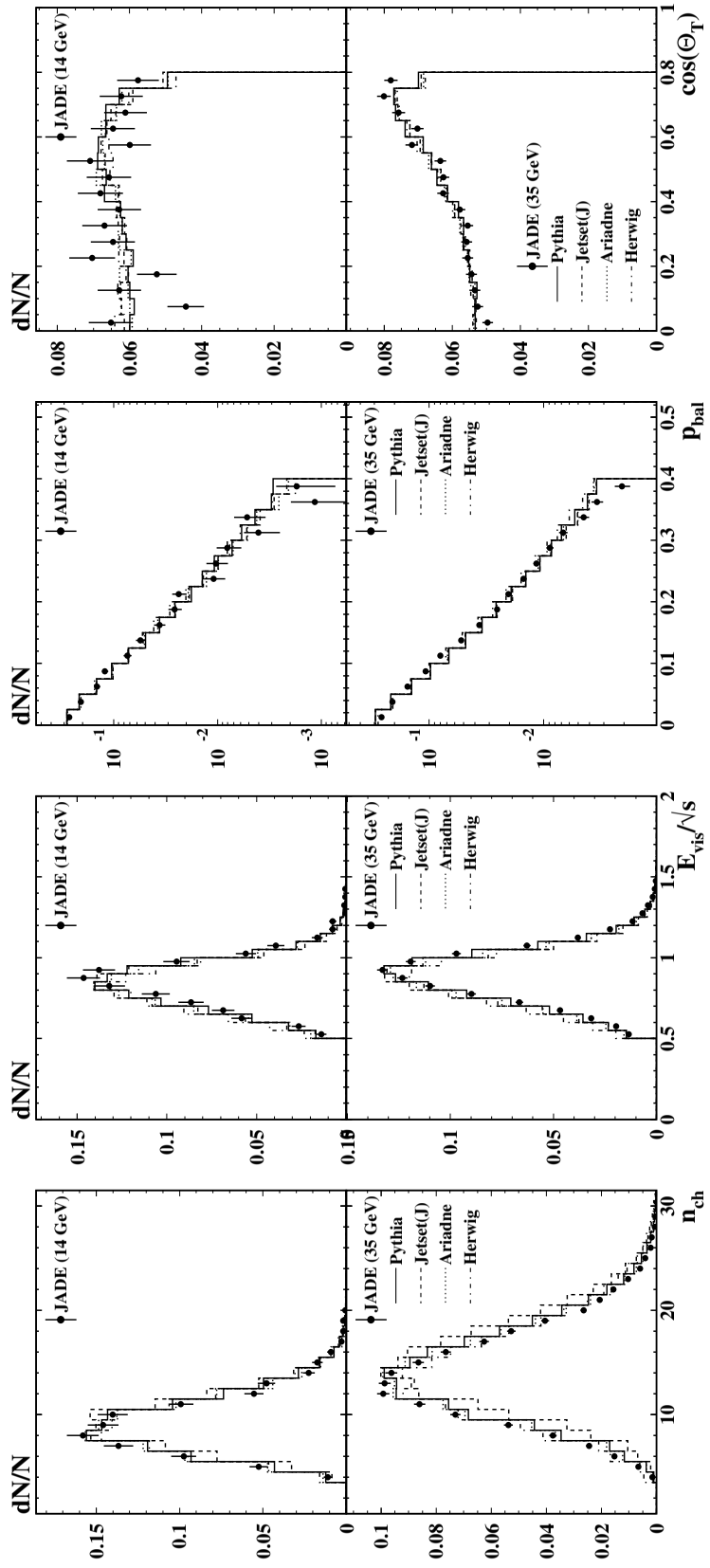

Figure 1: Normalised distributions of some multihadronic selection cut variables. Shown are the charged multiplicity $n_{\rm ch}$, the normalised visible energy $E_{\rm vis}/\sqrt{s}$, the momentum balance $p_{\rm bal}$ and the $\cos\theta_T$ distribution at $\sqrt{s} = 14$ and 35 GeV (tracking '86) in comparison with the JADE simulation based on various QCD event generators.

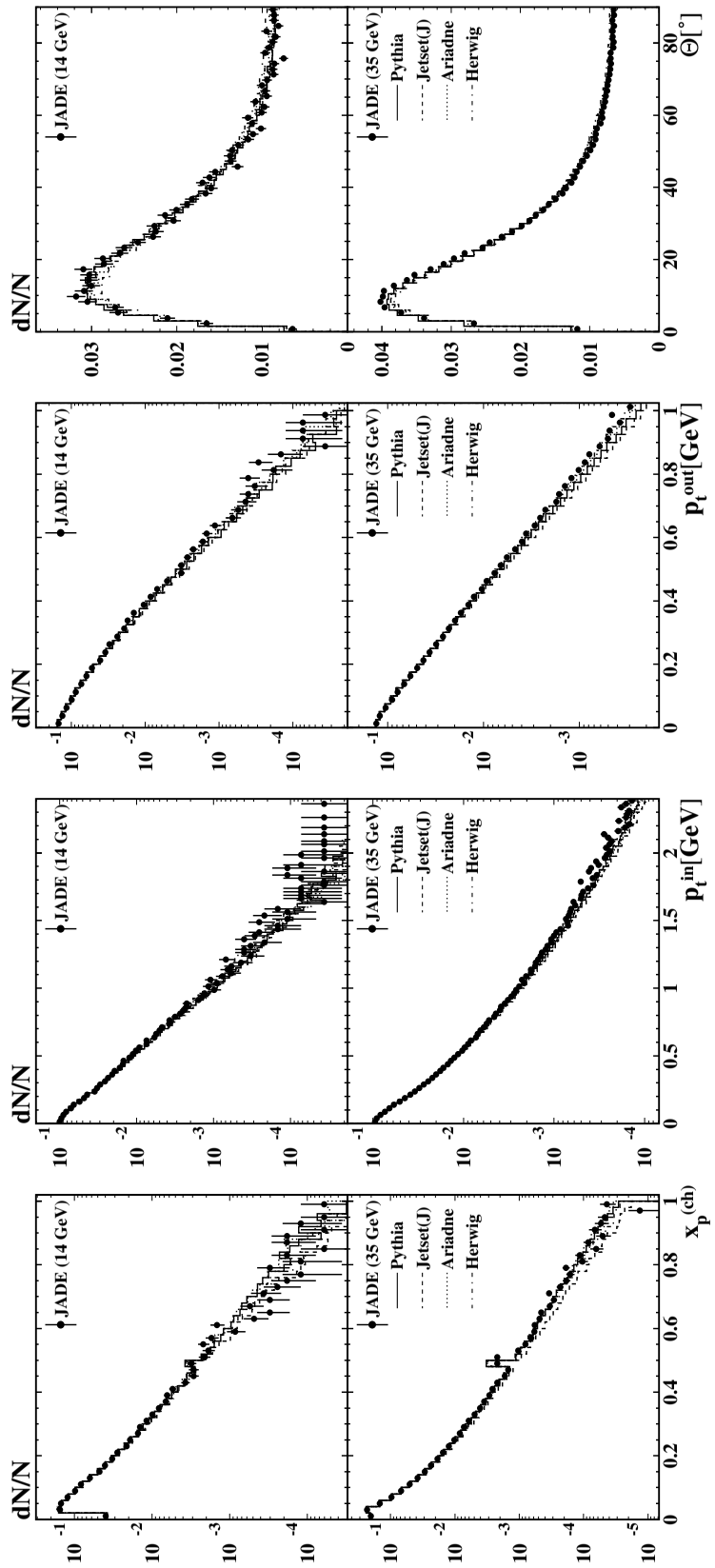

Figure 2: Normalised particle spectra at detector level. Shown are the charged particle momentum spectrum $x_p^{(\mathrm{ch})}$, the transverse momentum distribution w.r.t. to the sphericity axis within (p_t^{in}) and perpendicular to the event plane (p_t^{out}) and the particle flow w.r.t the thrust axis at $\sqrt{s} = 14$ and 35 GeV (tracking '86) in comparison with the JADE simulation based on various QCD event generators.

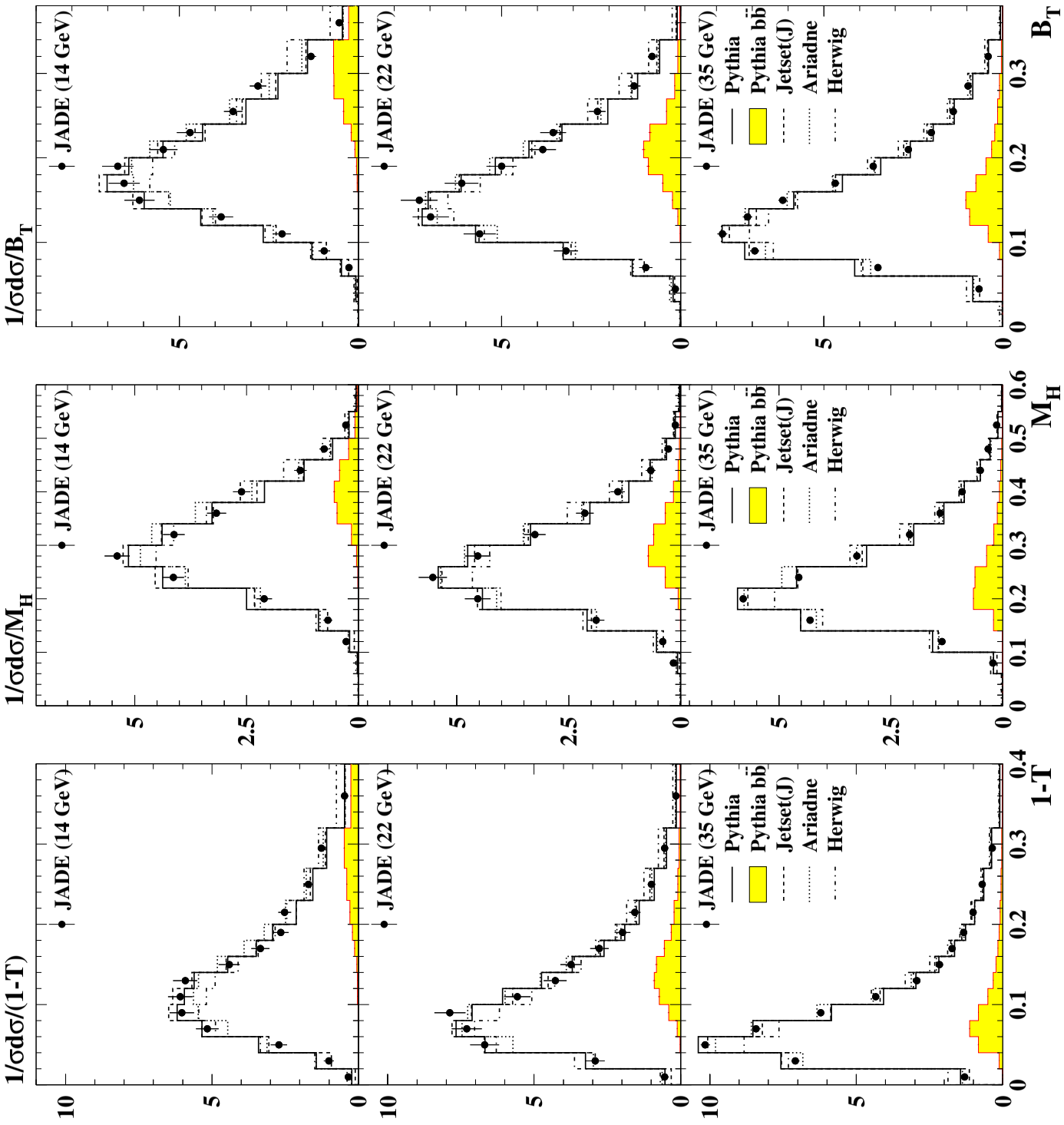

Figure 3: Normalised distributions of $1-T$, M_H and B_T at detector level compared with the JADE simulation at $\sqrt{s} = 14$ GeV, 22 GeV and 35 GeV (tracking '86) based on various QCD event generators. The error bars denote the statistical uncertainties. The shaded areas indicate the fraction of $b\bar{b}$ events estimated using PYTHIA.

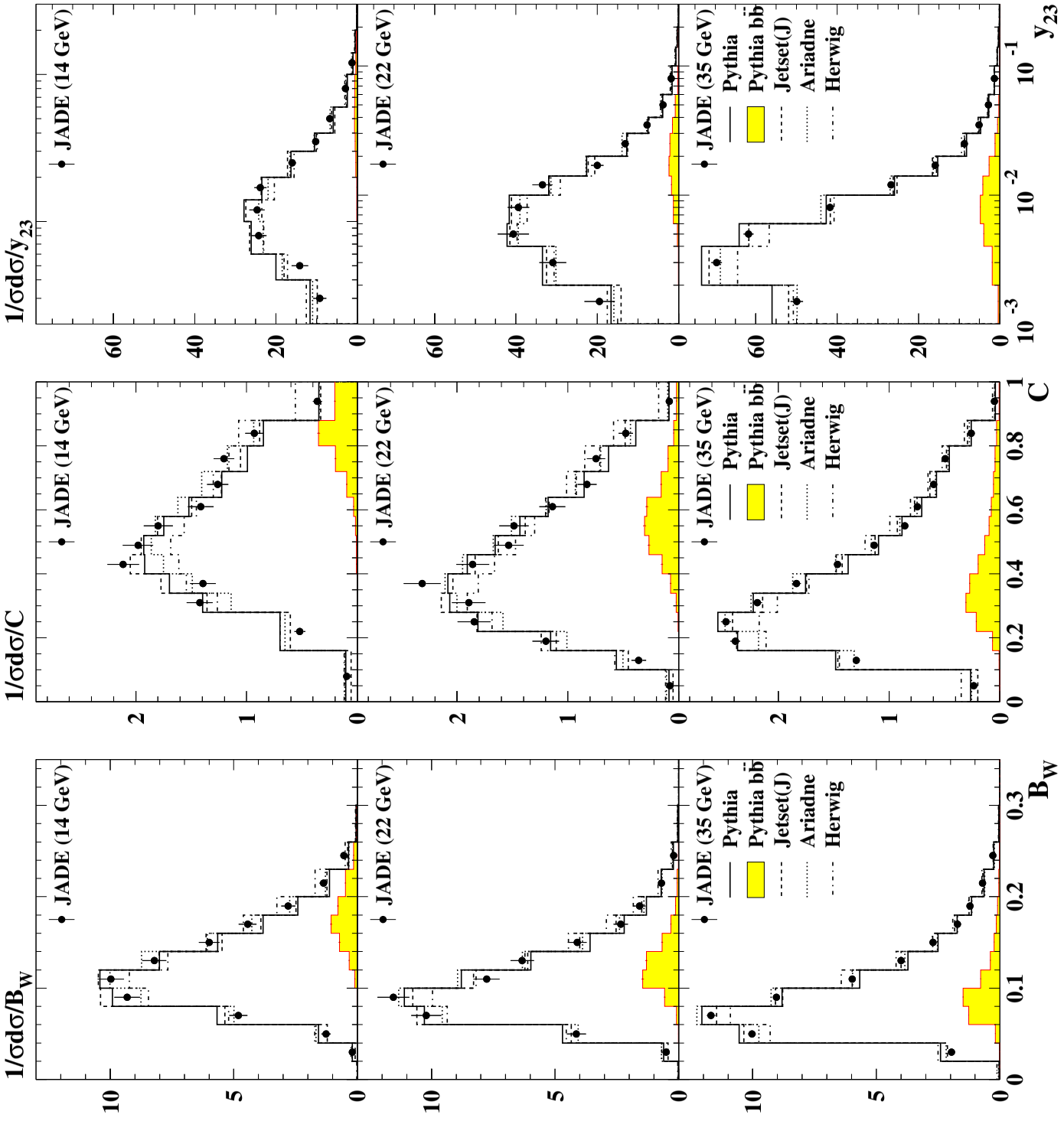

Figure 4: Normalised distributions of B_W, C and y_{23} at detector level compared with the JADE simulation at $\sqrt{s}$ = 14 GeV, 22 GeV and 35 GeV (tracking '86) based on various QCD event generators. The error bars denote the statistical uncertainties. The shaded areas indicate the fraction of $b\bar{b}$ events estimated using PYTHIA.

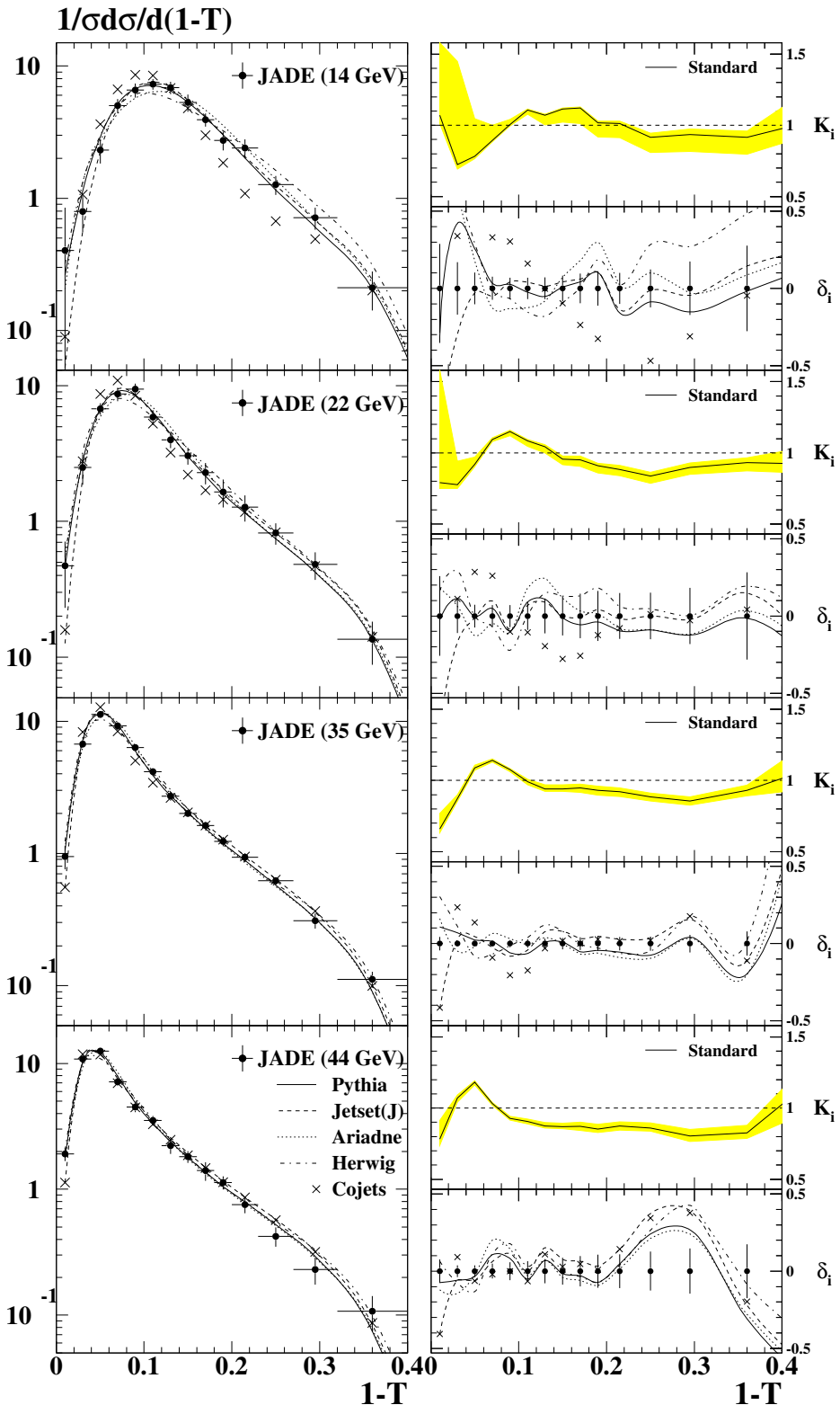

Figure 5: Normalised distributions of $1-T$ at hadron level at $\sqrt{s}$ = 14, 22, 35 (tracking '86) and 43.8 GeV (left). The error bars denote the statistical and systematic uncertainties added in quadrature. Predictions of PYTHIA, ARIADNE, JETSET(J), HERWIG and COJETS are shown using lines and markers of different styles. The diagrams on the righthand side show the detector correction factors $K_i = \sigma_i^{\rm had}/\sigma_i^{\rm det}$ for each bin i together with the correction uncertainties (shaded band) and the normalised difference between predictions and the data, $\delta_i = (\sigma_i^{\rm MC} - \sigma_i^{\rm dat})/\sigma_i^{\rm dat}$, in comparison with the total error.

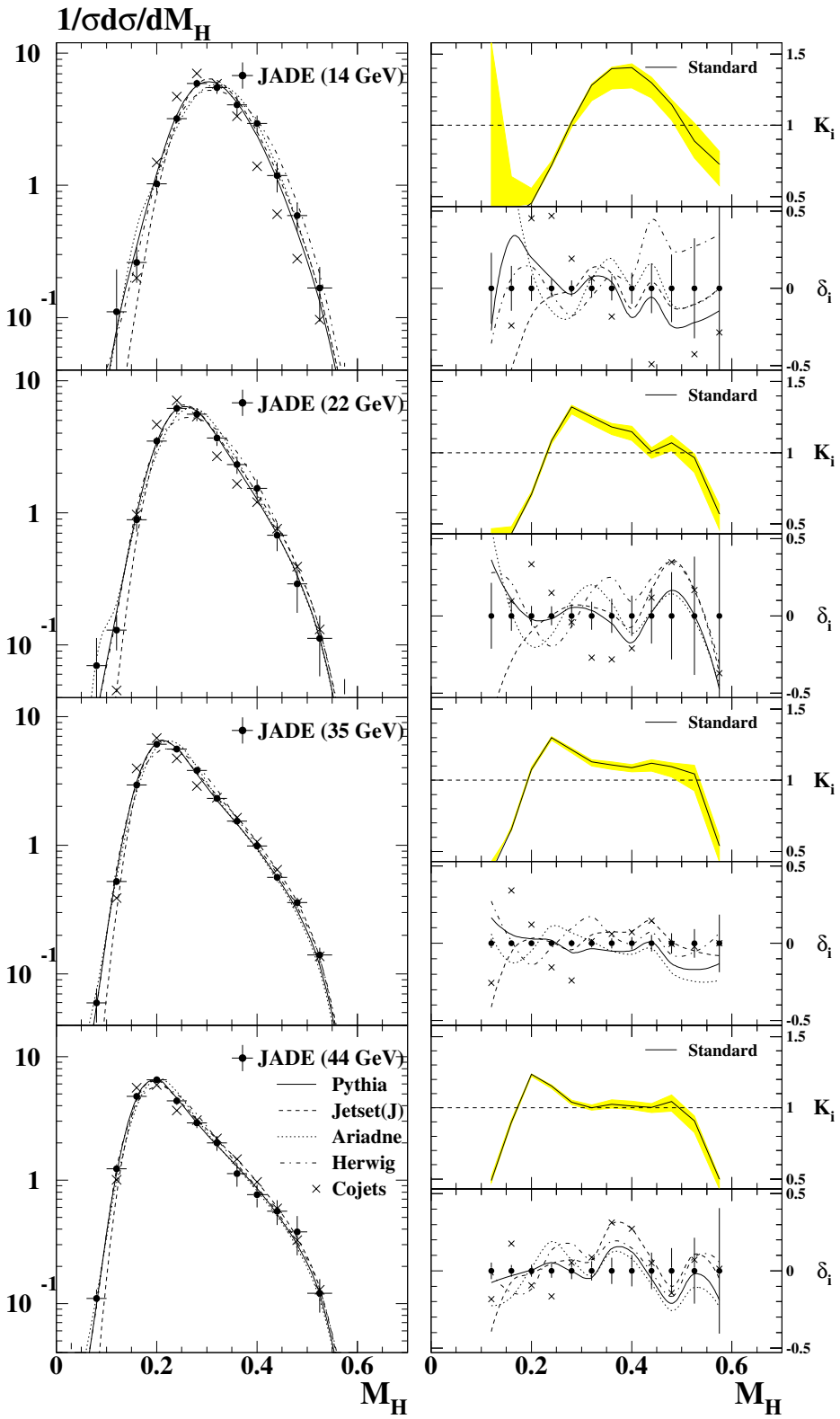

Figure 6: Normalised distributions of M_H at hadron level at $\sqrt{s} = 14$, 22, 35 (tracking '86) and 43.8 GeV (left). The error bars denote the statistical and systematic uncertainties added in quadrature. Predictions of PYTHIA, ARIADNE, JETSET(J), HERWIG and COJETS are shown using lines and markers of different styles. The diagrams on the righthand side show the detector correction factors $K_i = \sigma_i^{\rm had}/\sigma_i^{\rm det}$ for each bin i together with the correction uncertainties (shaded band) and the normalised difference between predictions and the data, $\delta_i = (\sigma_i^{\rm MC} - \sigma_i^{\rm dat})/\sigma_i^{\rm dat}$, in comparison with the total error.

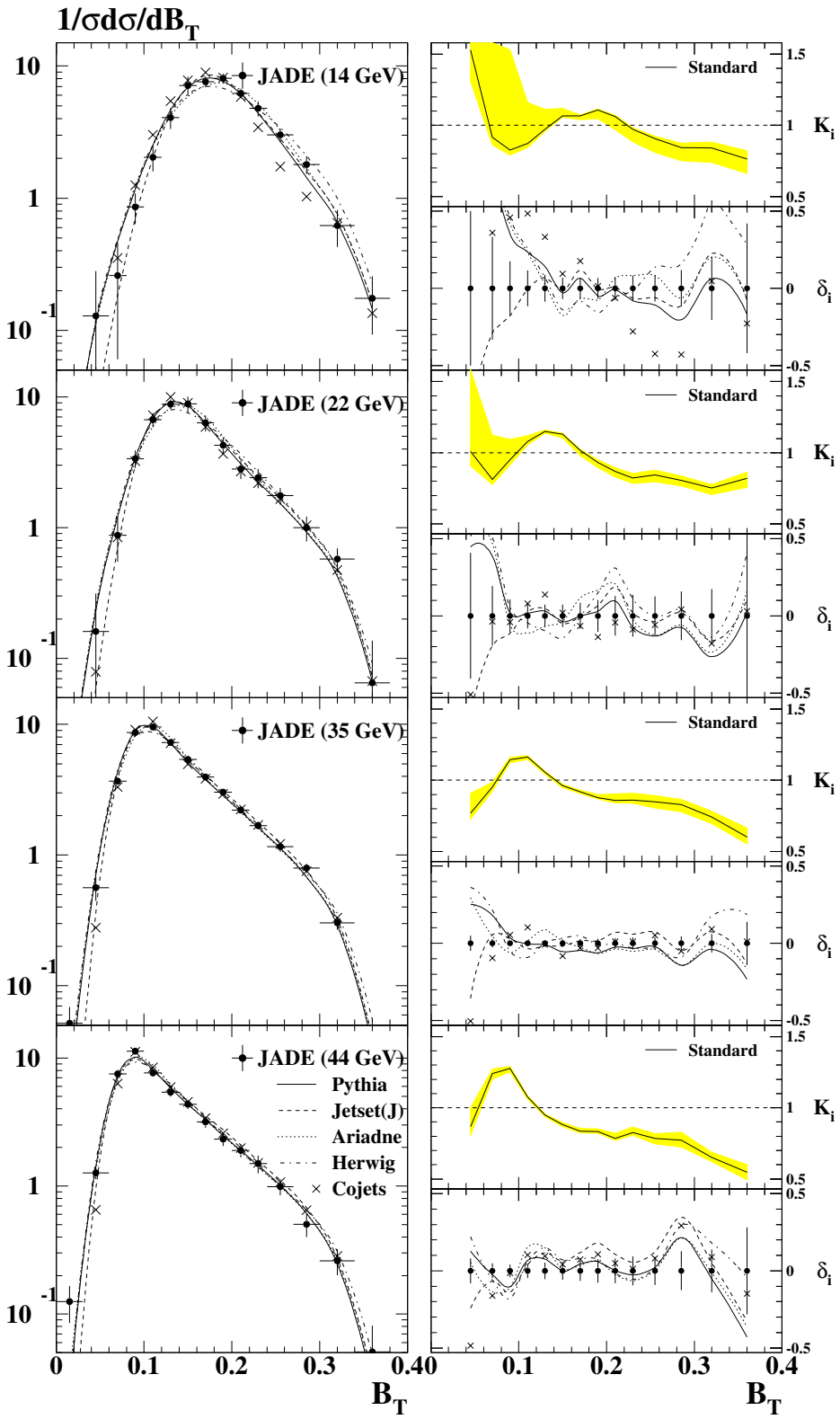

Figure 7: Normalised distributions of B_T at hadron level at $\sqrt{s} = 14, 22, 35$ (tracking '86) and 43.8 GeV (left). The error bars denote the statistical and systematic uncertainties added in quadrature. Predictions of PYTHIA, ARIADNE, JETSET(J), HERWIG and COJETS are shown using lines and markers of different styles. The diagrams on the righthand side show the detector correction factors $K_i = \sigma_i^{\rm had}/\sigma_i^{\rm det}$ for each bin i together with the correction uncertainties (shaded band) and the normalised difference between predictions and the data, $\delta_i = (\sigma_i^{\rm MC} - \sigma_i^{\rm dat})/\sigma_i^{\rm dat}$, in comparison with the total error.

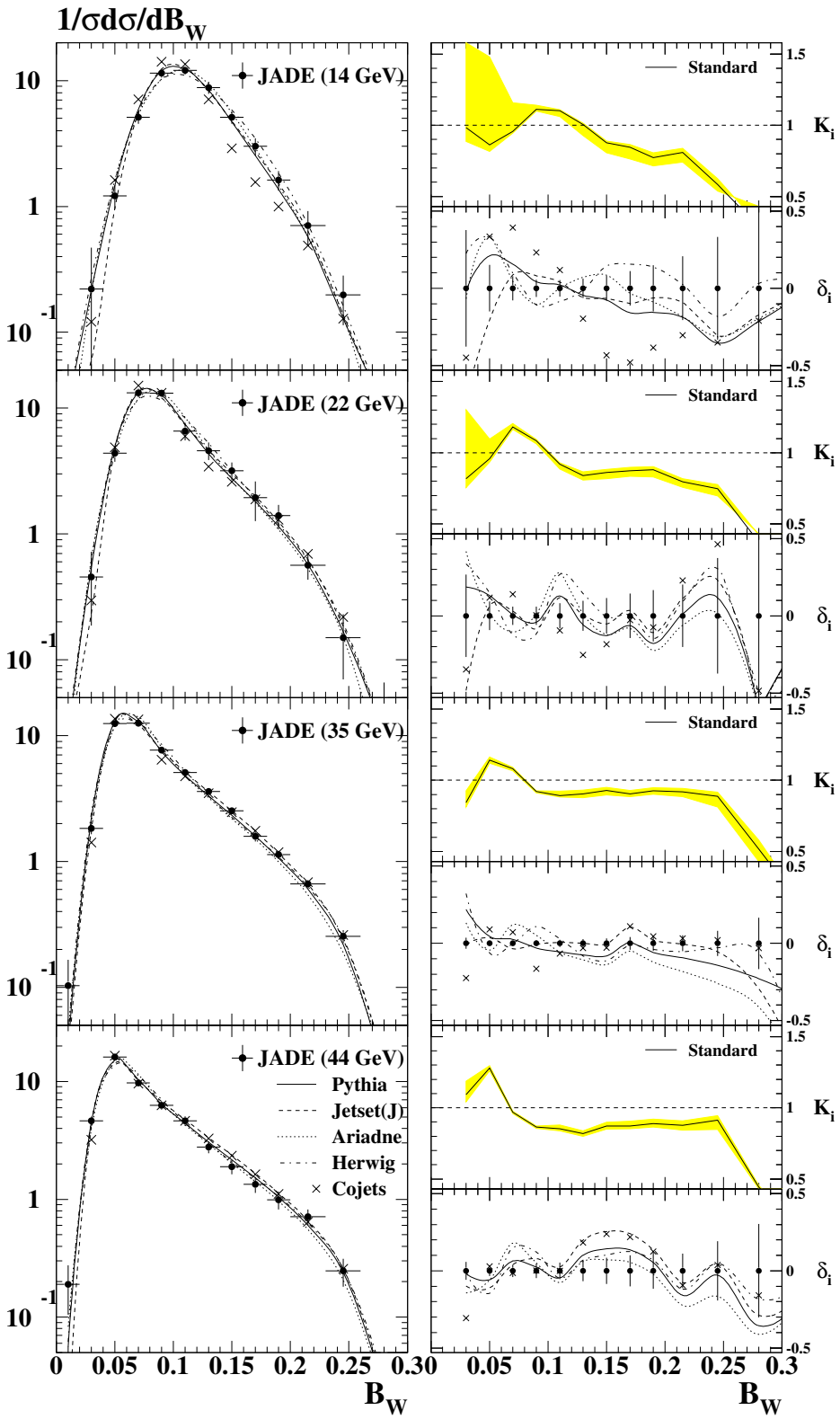

Figure 8: Normalised distributions of B_W at hadron level at $\sqrt{s} = 14$, 22, 35 (tracking '86) and 43.8 GeV (left). The error bars denote the statistical and systematic uncertainties added in quadrature. Predictions of PYTHIA, ARIADNE, JETSET(J), HERWIG and COJETS are shown using lines and markers of different styles. The diagrams on the righthand side show the detector correction factors $K_i = \sigma_i^{\rm had}/\sigma_i^{\rm det}$ for each bin i together with the correction uncertainties (shaded band) and the normalised difference between predictions and the data, $\delta_i = (\sigma_i^{\rm MC} - \sigma_i^{\rm dat})/\sigma_i^{\rm dat}$, in comparison with the total error.

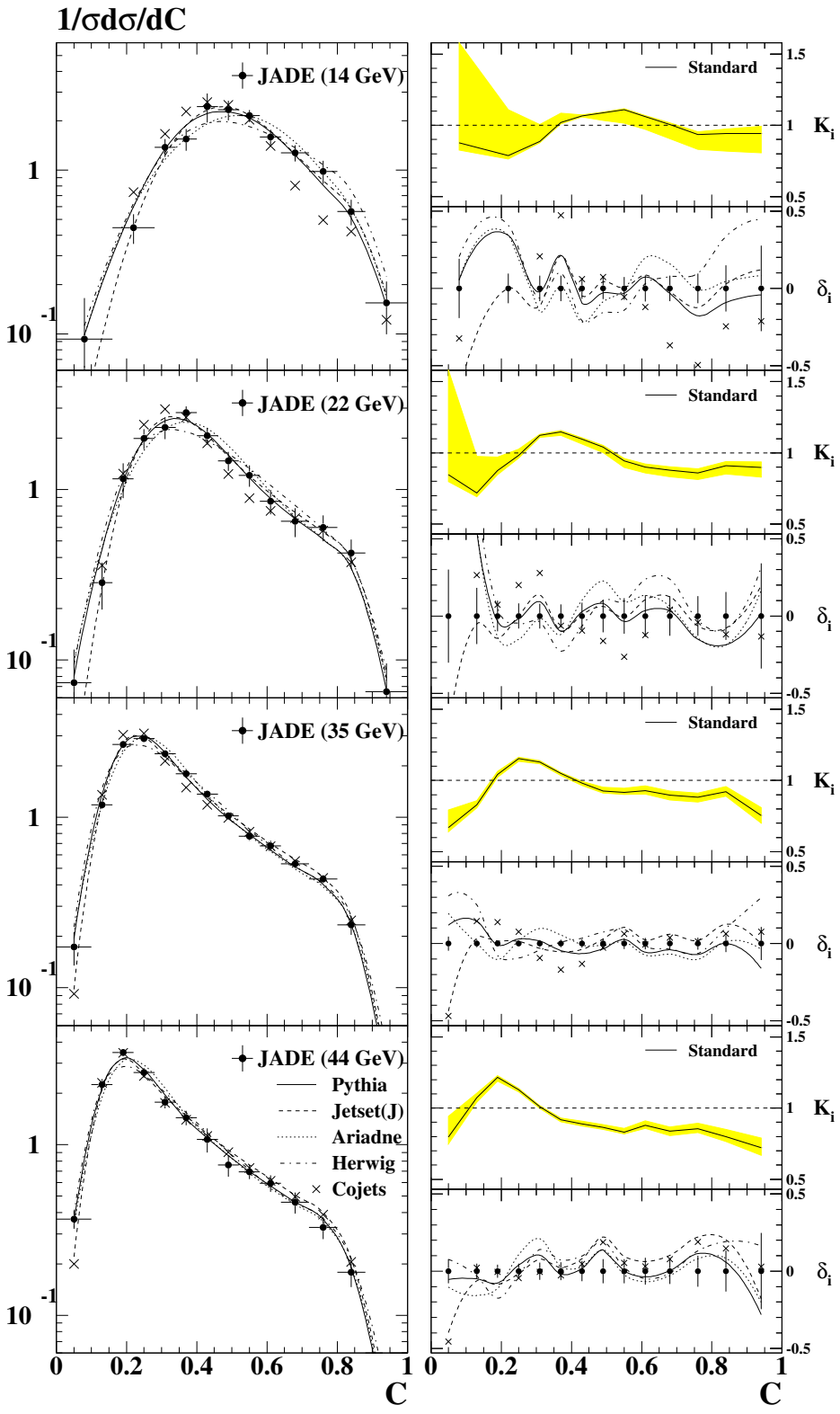

Figure 9: Normalised distributions of C at hadron level at $\sqrt{s} = 14$, 22, 35 (tracking '86) and 43.8 GeV (left). The error bars denote the statistical and systematic uncertainties added in quadrature. Predictions of PYTHIA, ARIADNE, JETSET(J), HERWIG and COJETS are shown using lines and markers of different styles. The diagrams on the righthand side show the detector correction factors $K_i = \sigma_i^{\rm had}/\sigma_i^{\rm det}$ for each bin i together with the correction uncertainties (shaded band) and the normalised difference between predictions and the data, $\delta_i = (\sigma_i^{\rm MC} - \sigma_i^{\rm dat})/\sigma_i^{\rm dat}$, in comparison with the total error.

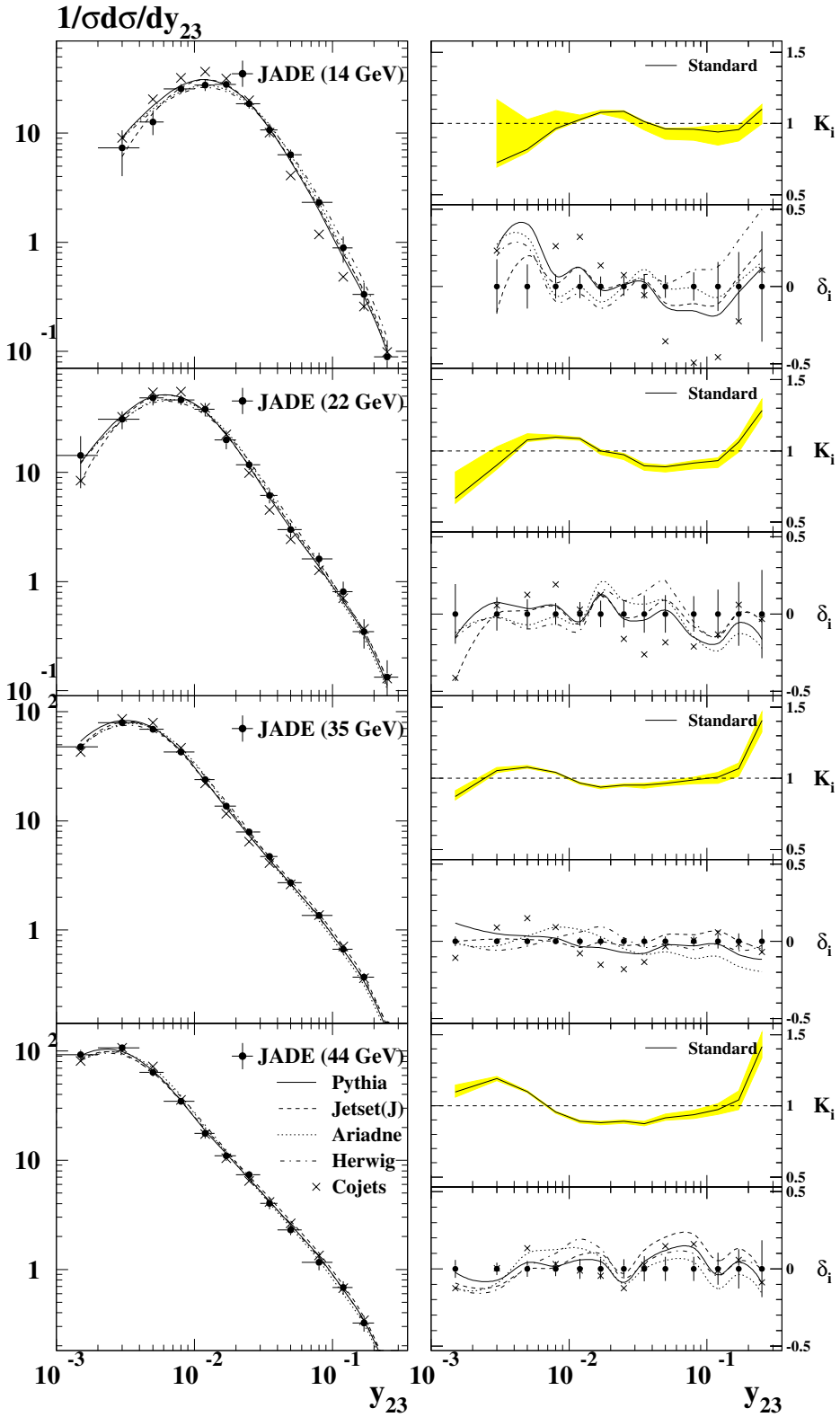

Figure 10: Normalised distributions of y_{23} at hadron level at $\sqrt{s} = 14$, 22, 35 (tracking '86) and 43.8 GeV (left). The error bars denote the statistical and systematic uncertainties added in quadrature. Predictions of PYTHIA, ARIADNE, JETSET(J), HERWIG and COJETS are shown using lines and markers of different styles. The diagrams on the righthand side show the detector correction factors $K_i = \sigma_i^{\rm had}/\sigma_i^{\rm det}$ for each bin i together with the correction uncertainties (shaded band) and the normalised difference between predictions and the data, $\delta_i = (\sigma_i^{\rm MC} - \sigma_i^{\rm dat})/\sigma_i^{\rm dat}$, in comparison with the total error.

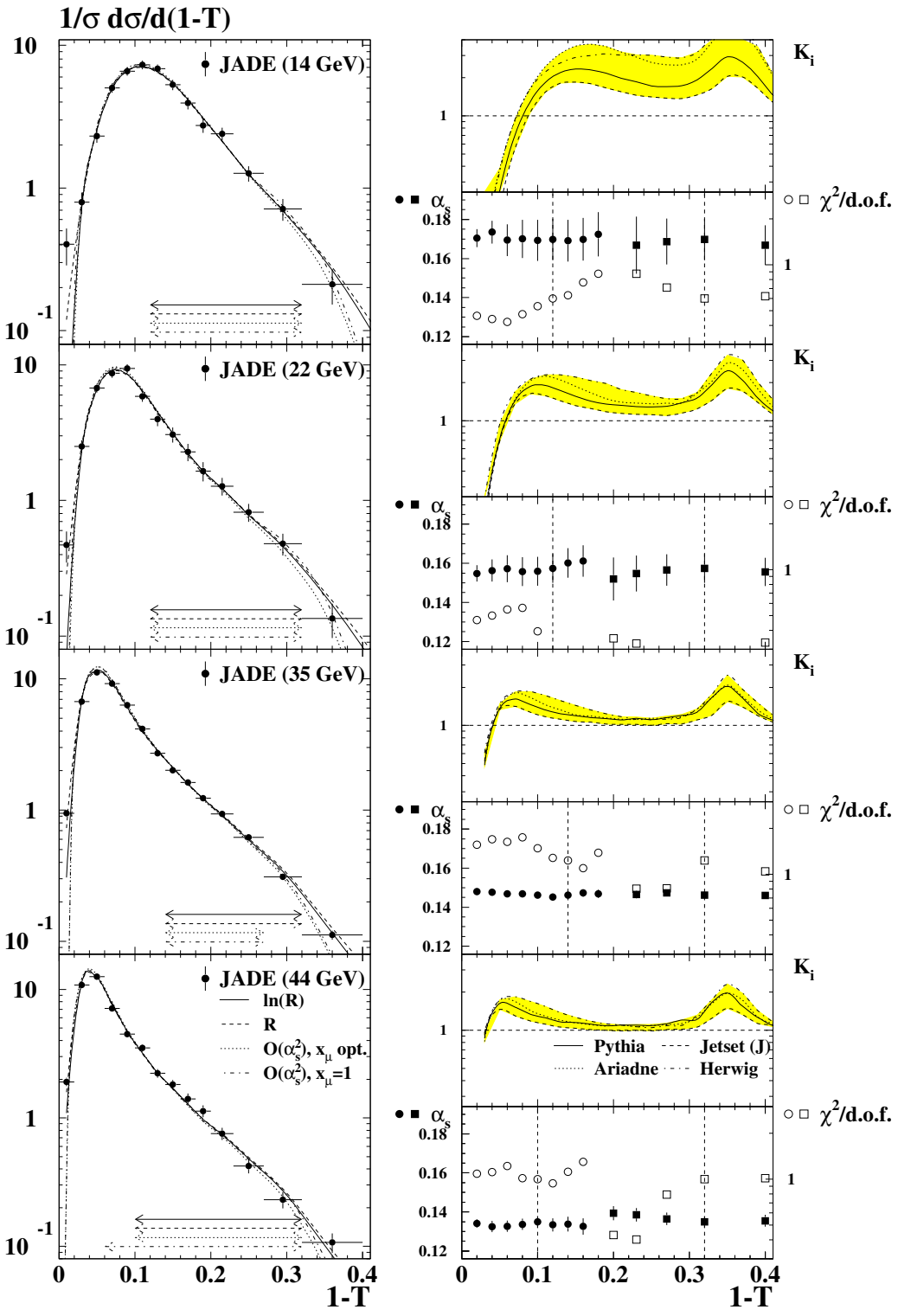

Figure 11: Fit of various QCD calculations to the hadron level measurements of $1-T$ at $\sqrt{s} = 14$ GeV, 22 GeV, 35 GeV (tracking '86) and 43.8 GeV (left). The error bars on the data represent the statistical uncertainties. The arrows indicate the fit ranges used for the different predictions. On the righthand side, the ratio $K_i = \sigma_i^{(\mathrm{pQCD+hadr.})}/\sigma_i^{(\mathrm{pQCD})}$ for each bin i derived from the cumulative cross sections $R(\mathcal{F}) = \int \mathrm{d}\mathcal{F}1/\sigma\,\mathrm{d}\sigma/\mathrm{d}\mathcal{F}$ of the predictions including (pQCD+hadr.) and excluding hadronisation effects (pQCD) are given by the smooth curves for various Monte Carlo models, together with the total hadronisation uncertainties represented by the shaded bands. The dependence of the results for α_S (solid symbols) and the χ^2/d.o.f. (open symbols) on the variation of the lower or the upper fit range is also shown.

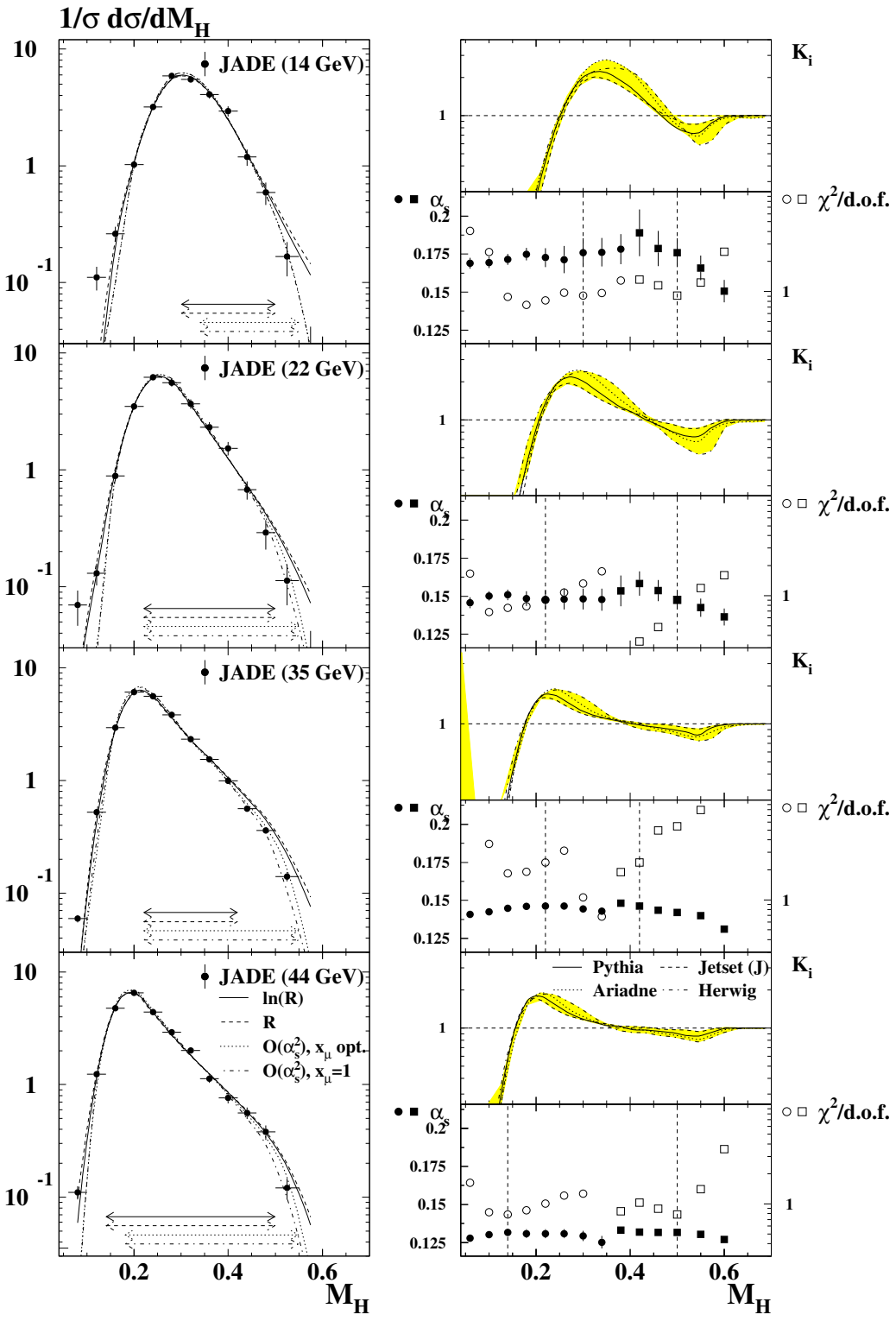

Figure 12: Fit of various QCD calculations to the hadron level measurements of M_H at $\sqrt{s} = 14$ GeV, 22 GeV, 35 GeV (tracking '86) and 43.8 GeV (left). The error bars on the data represent the statistical uncertainties. The arrows indicate the fit ranges used for the different predictions. On the righthand side, the ratio $K_i = \sigma_i^{(\mathrm{pQCD+hadr.})}/\sigma_i^{(\mathrm{pQCD})}$ for each bin i derived from the cumulative cross sections $R(\mathcal{F}) = \int \mathrm{d}\mathcal{F} 1/\sigma \mathrm{d}\sigma/\mathrm{d}\mathcal{F}$ of the predictions including (pQCD+hadr.) and excluding hadronisation effects (pQCD) are given by the smooth curves for various Monte Carlo models, together with the total hadronisation uncertainties represented by the shaded bands. The dependence of the results for α_S (solid symbols) and the χ^2/d.o.f. (open symbols) on the variation of the lower or the upper fit range is also shown.

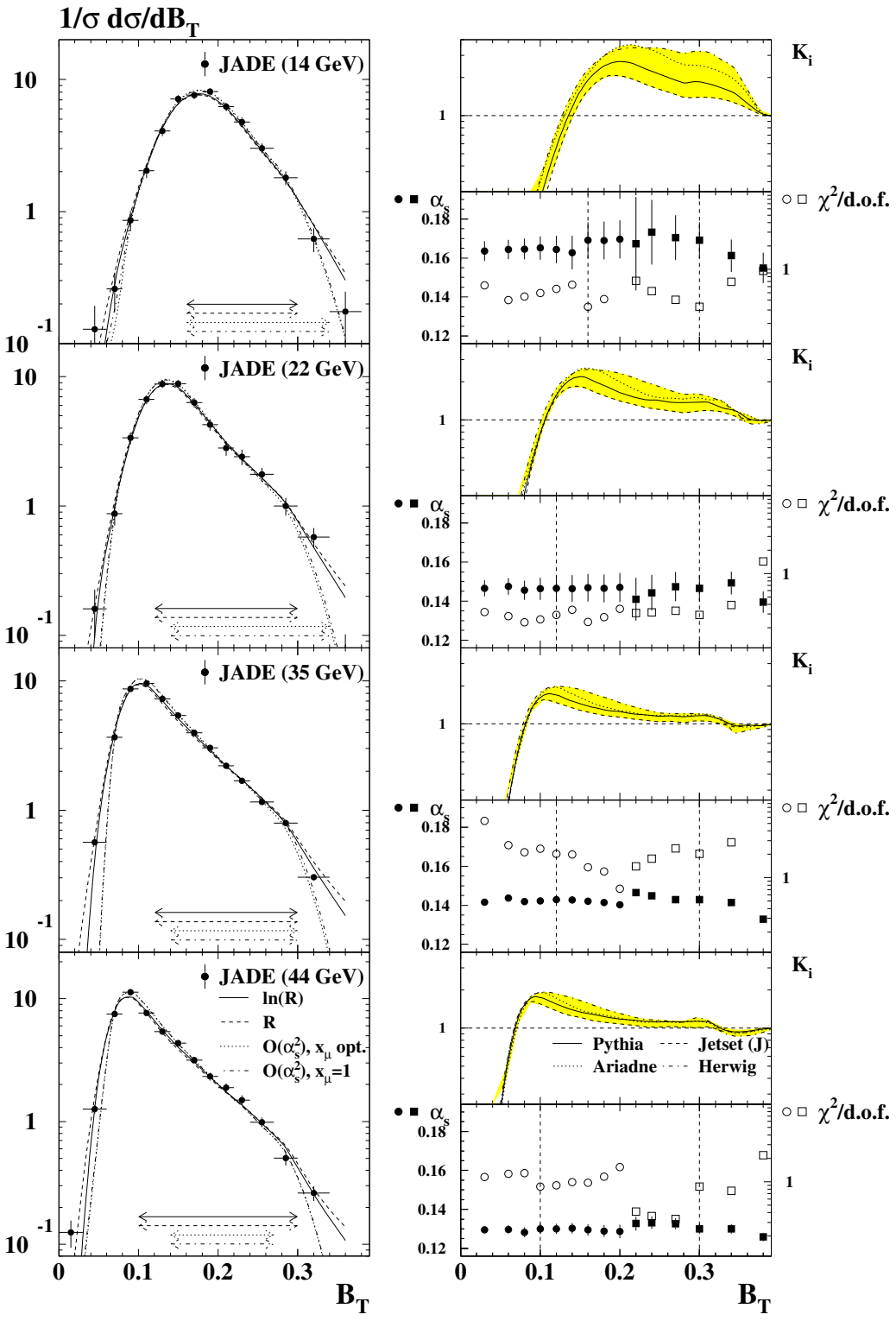

Figure 13: Fit of various QCD calculations to the hadron level measurements of B_T at $\sqrt{s} = 14$ GeV, 22 GeV, 35 GeV (tracking '86) and 43.8 GeV (left). The error bars on the data represent the statistical uncertainties. The arrows indicate the fit ranges used for the different predictions. On the righthand side, the ratio $K_i = \sigma_i^{(\mathrm{pQCD+hadr.})}/\sigma_i^{(\mathrm{pQCD})}$ for each bin i derived from the cumulative cross sections $R(\mathcal{F}) = \int \mathrm{d}\mathcal{F} 1/\sigma \mathrm{d}\sigma/\mathrm{d}\mathcal{F}$ of the predictions including (pQCD+hadr.) and excluding hadronisation effects (pQCD) are given by the smooth curves for various Monte Carlo models, together with the total hadronisation uncertainties represented by the shaded bands. The dependence of the results for α_S (solid symbols) and the χ^2/d.o.f. (open symbols) on the variation of the lower or the upper fit range is also shown.

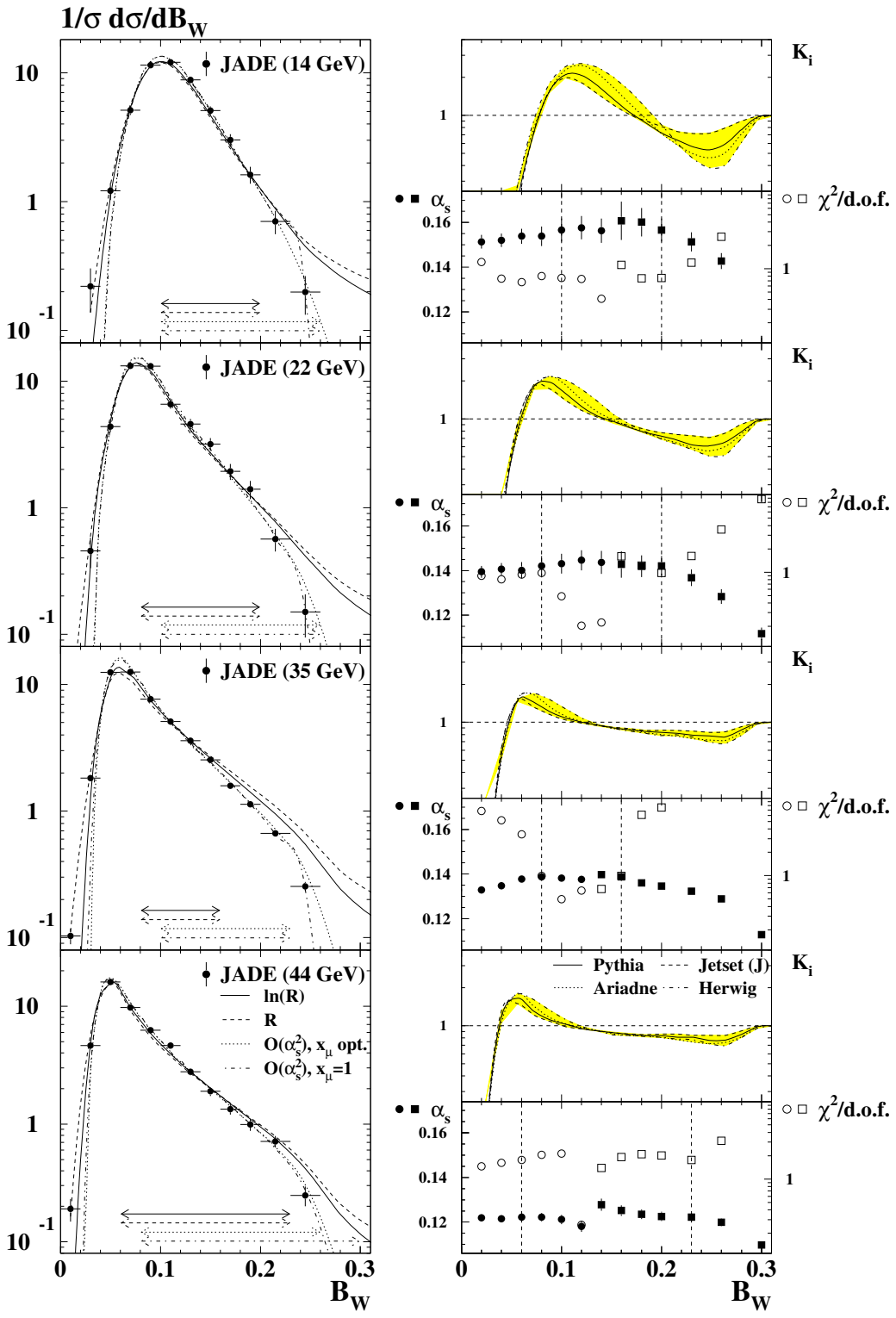

Figure 14: Fit of various QCD calculations to the hadron level measurements of B_W at $\sqrt{s} = 14$ GeV, 22 GeV, 35 GeV (tracking '86) and 43.8 GeV (left). The error bars on the data represent the statistical uncertainties. The arrows indicate the fit ranges used for the different predictions. On the righthand side, the ratio $K_i = \sigma_i^{(\mathrm{pQCD+hadr.})}/\sigma_i^{(\mathrm{pQCD})}$ for each bin i derived from the cumulative cross sections $R(\mathcal{F}) = \int \mathrm{d}\mathcal{F}1/\sigma \mathrm{d}\sigma/\mathrm{d}\mathcal{F}$ of the predictions including (pQCD+hadr.) and excluding hadronisation effects (pQCD) are given by the smooth curves for various Monte Carlo models, together with the total hadronisation uncertainties represented by the shaded bands. The dependence of the results for α_S (solid symbols) and the χ^2/d.o.f. (open symbols) on the variation of the lower or the upper fit range is also shown.

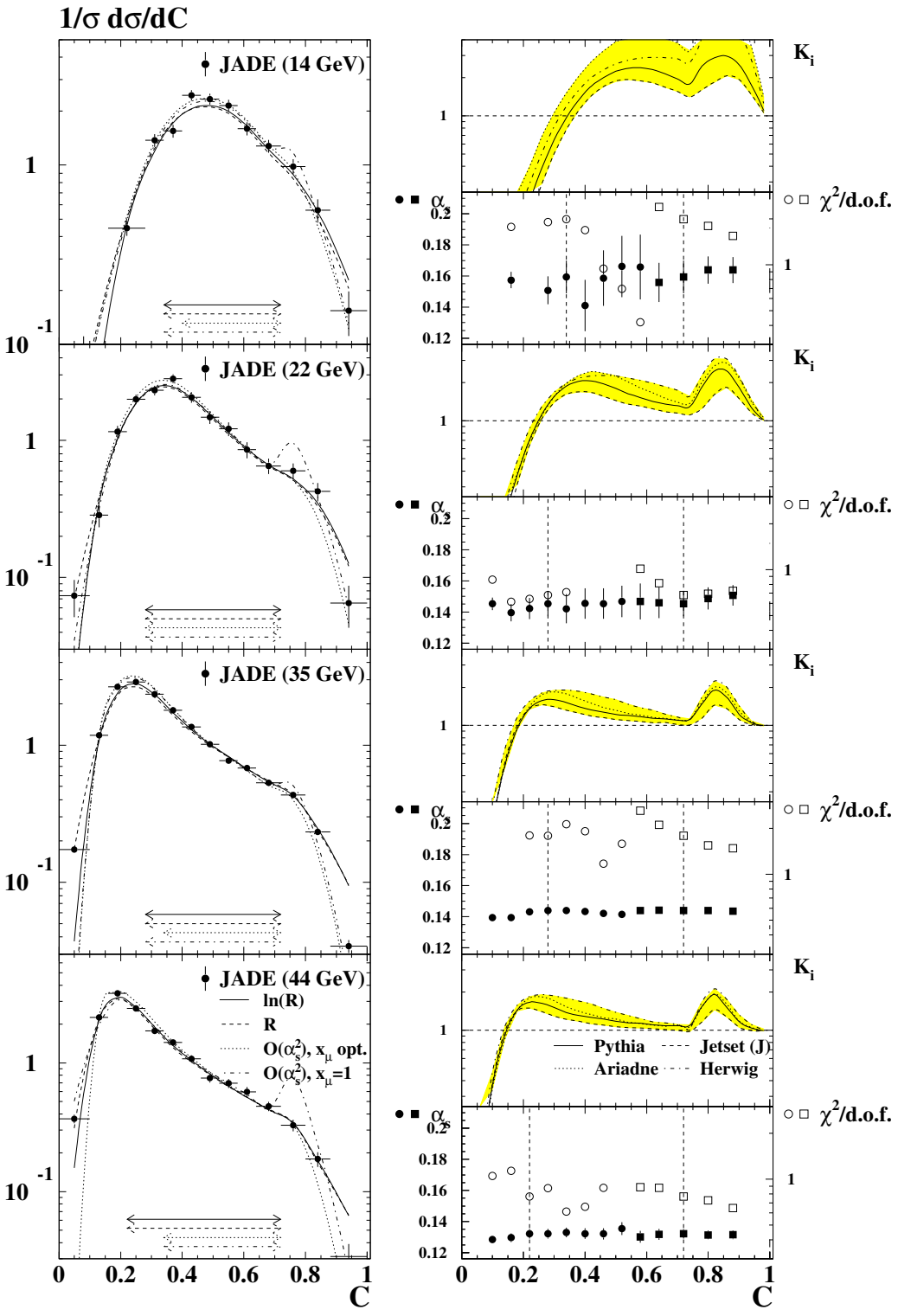

Figure 15: Fit of various QCD calculations to the hadron level measurements of C at $\sqrt{s} = 14$ GeV, 22 GeV, 35 GeV (tracking '86) and 43.8 GeV (left). The error bars on the data represent the statistical uncertainties. The arrows indicate the fit ranges used for the different predictions. On the righthand side, the ratio $K_i = \sigma_i^{(\mathrm{pQCD+hadr.})}/\sigma_i^{(\mathrm{pQCD})}$ for each bin i derived from the cumulative cross sections $R(\mathcal{F}) = \int \mathrm{d}\mathcal{F} 1/\sigma \mathrm{d}\sigma/\mathrm{d}\mathcal{F}$ of the predictions including (pQCD+hadr.) and excluding hadronisation effects (pQCD) are given by the smooth curves for various Monte Carlo models, together with the total hadronisation uncertainties represented by the shaded bands. The dependence of the results for α_S (solid symbols) and the χ^2/d.o.f. (open symbols) on the variation of the lower or the upper fit range is also shown.

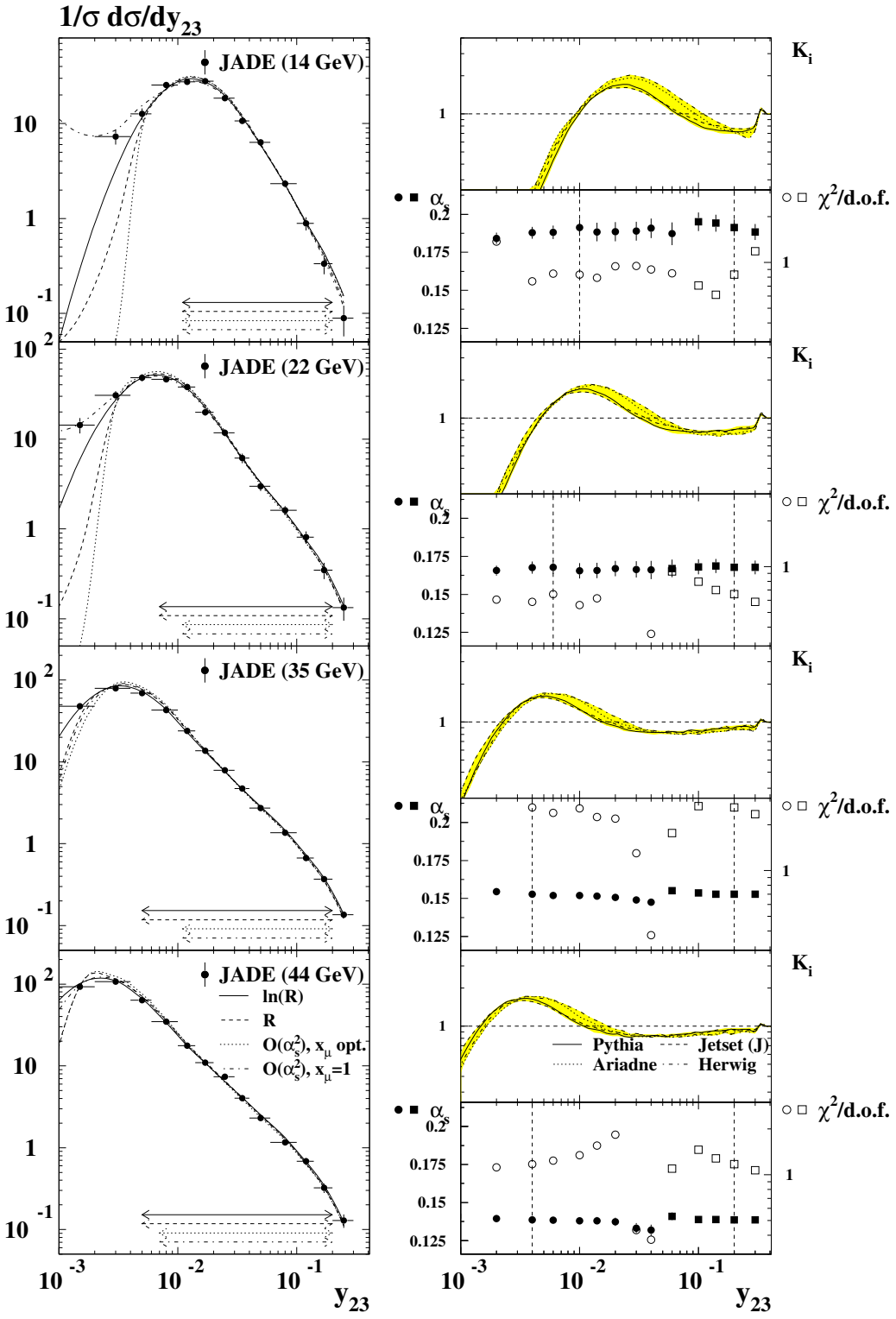

Figure 16: Fit of various QCD calculations to the hadron level measurements of y_{23} at $\sqrt{s} = 14$ GeV, 22 GeV, 35 GeV (tracking '86) and 43.8 GeV (left). The error bars on the data represent the statistical uncertainties. The arrows indicate the fit ranges used for the different predictions. On the righthand side, the ratio $K_i = \sigma_i^{(\mathrm{pQCD+hadr.})}/\sigma_i^{(\mathrm{pQCD})}$ for each bin i derived from the cumulative cross sections $R(\mathcal{F}) = \int \mathrm{d}\mathcal{F}1/\sigma \mathrm{d}\sigma/\mathrm{d}\mathcal{F}$ of the predictions including (pQCD+hadr.) and excluding hadronisation effects (pQCD) are given by the smooth curves for various Monte Carlo models, together with the total hadronisation uncertainties represented by the shaded bands. The dependence of the results for α_S (solid symbols) and the χ^2/d.o.f. (open symbols) on the variation of the lower or the upper fit range is also shown.

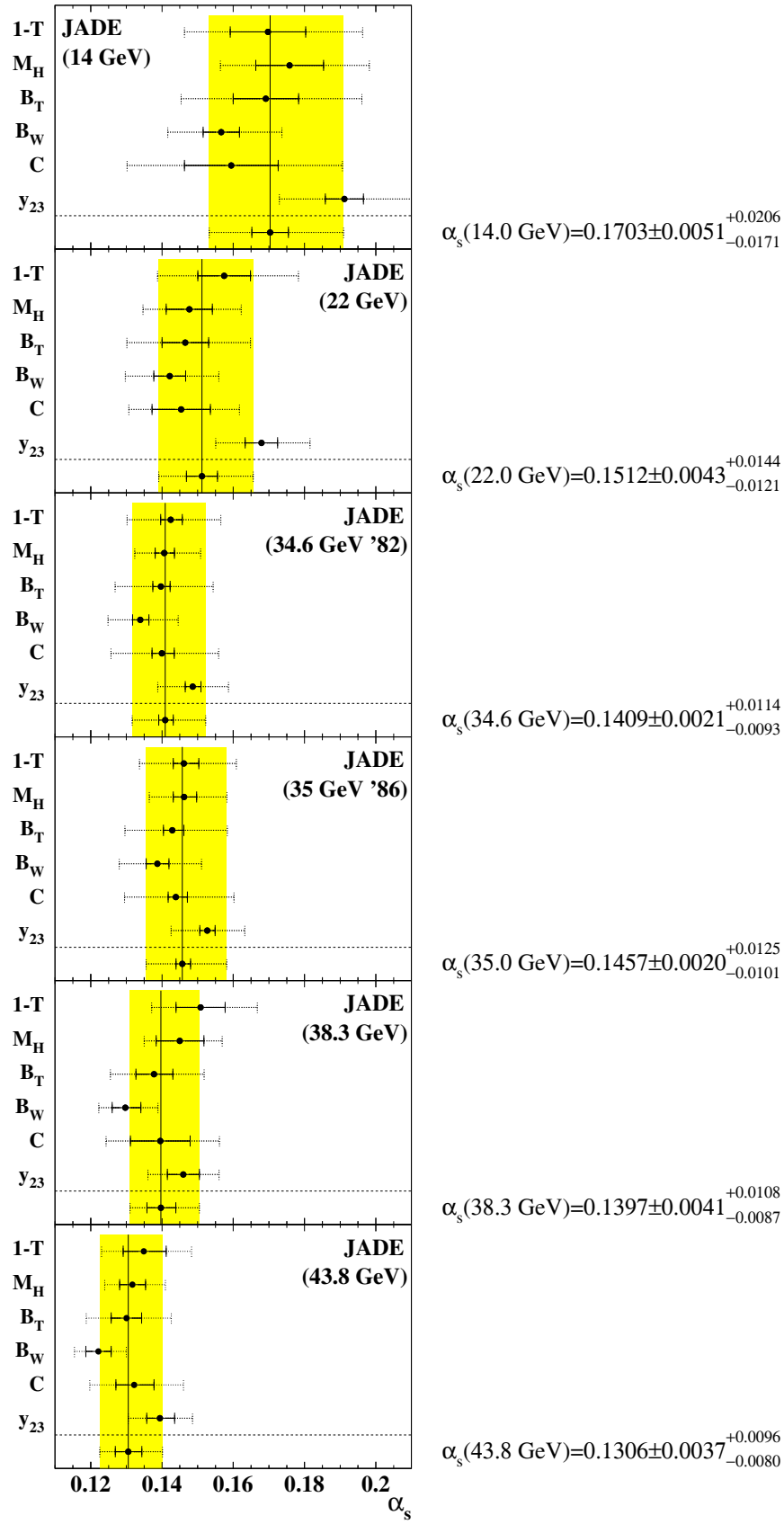

Figure 17: Results for $\alpha_S(\sqrt{s})$ at $\sqrt{s}$ =14.0, 22.0, 34.6 (tracking '82), 35.0 (tracking '86), 38.3 and 43.8 GeV derived from the comparison of $\mathcal{O}(\alpha_S^2)$+NLLA-predictions with event shape distributions for $1-T$, M_H, B_T, B_W, C and y_{23}. The inner error bars denote the quadratic sum of the statistical and experimental systematic uncertainties of the fits, the outer error bars are the total errors. The α_S result for a given centre-of-mass energy is calculated from the the individual results using the weighted mean method.

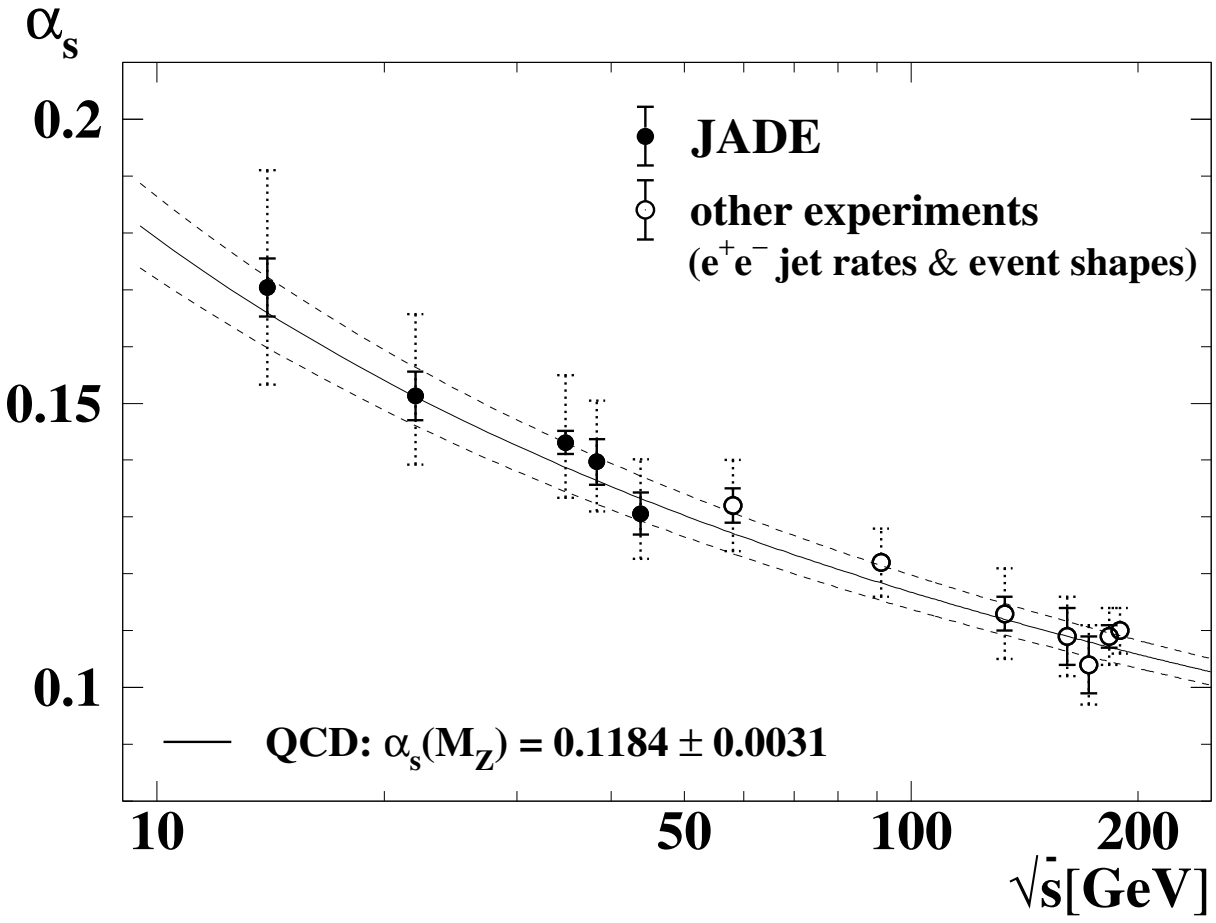

Figure 18: Values of α_S from $\mathcal{O}(\alpha_S^2)$+NLLA fits, as a function of the centre-of-mass energy $\sqrt{s}$. The solid error bars are the statistical and experimental uncertainties added in quadrature, the dotted error bars denote the total errors. The full points represent the values for α_S extracted from JADE data which are compared to the results obtained from other experiments [48] based on a similar set of event shape and jet rate observables. The solid and the dashed lines represent the QCD prediction for the world average value of the strong coupling constant, $\alpha_S(M_{Z^0}) = 0.118 \pm 0.003$ [48].